Gondwana Research 117 (2023) 207–229

Contents lists available at ScienceDirect

Gondwana Research

journal homepage: www.elsevier.com/locate/gr

Synchronous exhumation episodes across Arctic Canada, North Greenland and Svalbard in relation to the Eurekan Orogeny

Peter Japsen [a,*], Paul F. Green [b], James A. Chalmers [a]

[a] Geological Survey of Denmark and Greenland (GEUS), Øster Voldgade, 10, 1354 Copenhagen, Denmark
[b] Geotrack International, 1/11 Tullarmine Park Road, Tullamarine, Victoria 3043, Australia

ARTICLE INFO

Article history:
Received 10 September 2021
Revised 15 December 2022
Accepted 27 January 2023
Available online 1 February 2023
Handling Editor: Taras Gerya

Keywords:
Iceland Plume
Plate tectonics
Sverdrup Basin
Thermochronology
Wandel Sea Basin
West Spitsbergen Fold Belt

ABSTRACT

The sedimentary record across the Canadian High Arctic, North Greenland and Svalbard is fragmentary, making regional correlation difficult. We seek new insights by integrating information from the preserved geological section with evidence of former stratigraphic units that are no longer present (missing section), using paleo-thermal methods to define episodes of deeper burial and subsequent exhumation. Parts of the region were affected by deformation induced by the Paleocene–Eocene movement of Greenland relative to the North American and Eurasian plates (the Eurekan Orogeny). However, our results indicate four discrete episodes of kilometre-scale exhumation before, during and after the Eurekan Orogeny that led to disruption of sedimentary basins across the region. (1) Regional Maastrichtian exhumation possibly reflects doming above the rising Iceland Plume. The plume impact at the base of the lithosphere contributed to the onset of mid-Paleocene sea-floor spreading west of Greenland that provided the driving force for the Eurekan Orogeny. (2) Localized Paleocene exhumation was caused by inversion of fault zones in the initial stage of the Eurekan Orogeny due to compression that also formed foreland basins and caused the West Spitsbergen Fold Belt. (3) Regional exhumation that began at the end of the Eocene postdates sea-floor spreading west of Greenland and thus represents post-Eurekan tectonics. This episode, which also affected regions far from the Eurekan Orogen, coincided with a major change in the North-East Atlantic spreading system. Transmission of stress from a shift in the motion of Africa relative to Europe may have contributed to these changes. (4) Regional, late Miocene uplift and erosion initiated the development of present-day landscapes. Our results show both local uplift events within the Eurekan Orogen and synchronous effects over large regions that require new ideas about the stresses driving horizontal and vertical movements of the earth's crust.

1. Introduction

The sedimentary record across the Canadian High Arctic (north of 68°N), North Greenland and Svalbard is a puzzle of isolated components with significant variation of thermal maturity over short distances, overprinted by faults and thrusts during the Paleogene Eurekan Orogeny (Thorsteinsson and Tozer, 1970; Steel et al., 1985; Ricketts, 1994; Håkansson and Pedersen, 1982, 2015; Harrison and St-Onge, 2022; Oakey and Chalmers, 2012; Dallmann, 2015; Piepjohn et al., 2016; Jones et al., 2017; Dörr et al., 2018; Japsen et al., 2021a). Here we seek to provide a more complete understanding of the tectonic development of the region by integrating evidence from the preserved rock record with constraints from low-temperature thermochronology on thicknesses of rock that were once present but have since been removed (missing section; see Green et al., 2022a). We refer to this region as well as the Lomonosov Ridge and the Barents Sea as the High Arctic (Fig. 1).

To establish a coherent tectonic framework for understanding the processes that may have driven these exhumation episodes, we review the Paleogene plate-tectonic movements around the High Arctic (Fig. 2). After intra-continental extension both east and west of Greenland in the Mesozoic, sea-floor spreading moved Greenland relative to the North American and Eurasian plates in the Paleogene in three phases: Phase 1 in the late Paleocene, when Greenland moved together with Eurasia relative to North America, Phase 2 in the Eocene when Greenland moved relative to both Eurasia and North America and Phase 3 when Greenland together with North America moved relative to Eurasia (Oakey and Chalmers, 2012; Gaina et al., 2017). The sea-floor spreading movements resulted in transverse and compressional movements in northern

* Corresponding author.
E-mail address: pj@geus.dk (P. Japsen).

https://doi.org/10.1016/j.gr.2023.01.011
1342-937X/

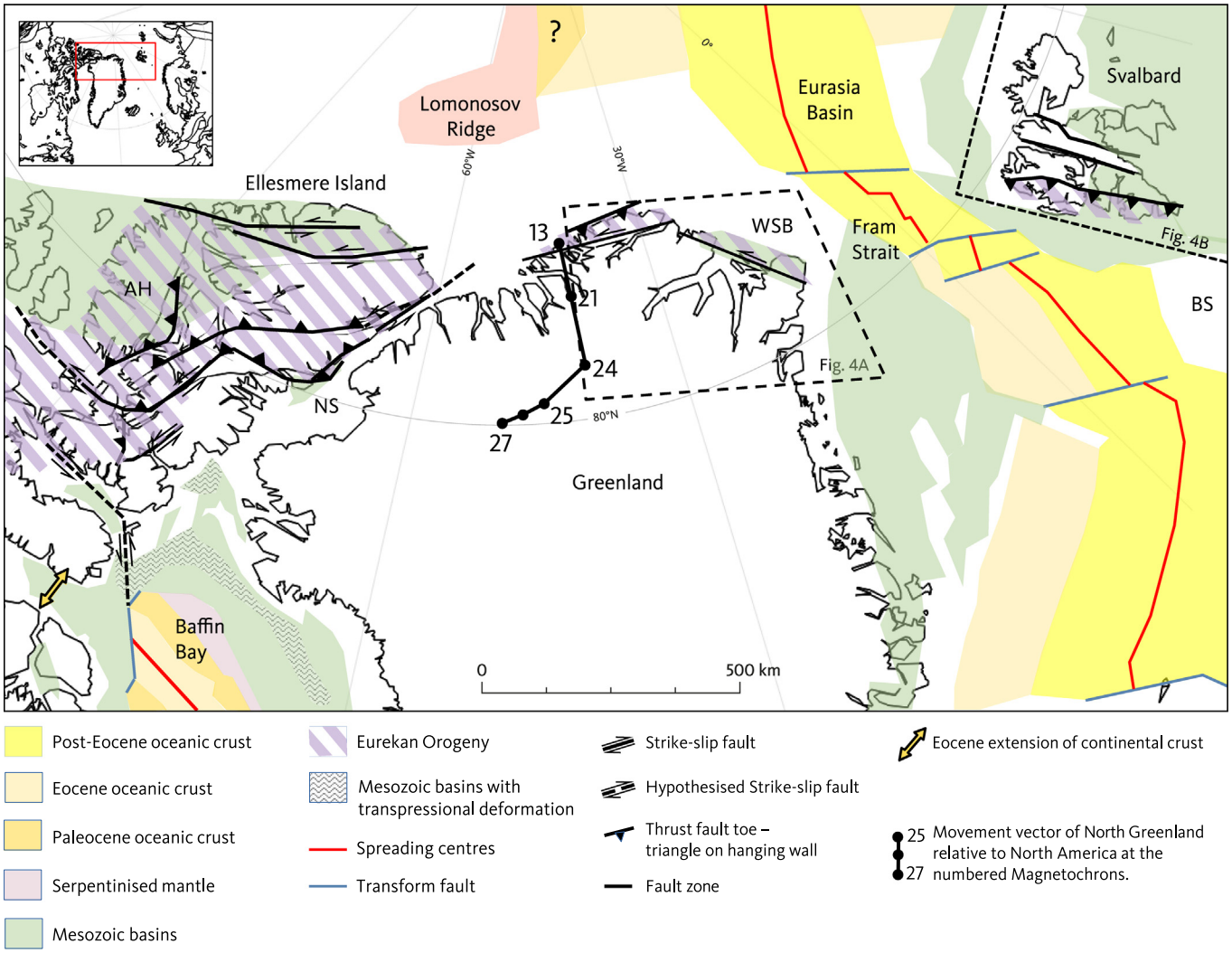

Fig. 1. Geological outline of the area around northern Greenland. Mesozoic extension around Greenland formed sedimentary basins. Sea-floor spreading started west of Greenland in the mid-Paleocene and east of Greenland in the early Eocene after which time the spreading direction of Greenland relative to North America changed. Vectors of this movement show where present-day locations on North Greenland were relative to the North American plate at C13 (33 Ma) and present-day, C21 (47 Ma), 24 (55 Ma), C25 (57 Ma) and C27 (62 Ma) (Oakey and Chalmers, 2012). Sea-floor spreading in the Eurasian Basin may have started in the late Paleocene (Brozena et al., 2003) or the early Eocene (Jokat et al., 2016). Areas affected by the Eurekan Orogeny are marked in purple. AH: Axel Heiberg Island. BS: Barents Shelf. HFFZ: Harder Fjord Fault Zone. KCTZ: Kap Cannon Thrust Zone. NS: Nares Strait. TLFZ: Trolle Land Fault Zone. WSB: Wandel Sea Basin (Greenland north of 80°N, east of 40°W). Compiled from: Brozena et al. (2003), Dallmann (2015), Faleide et al. (2008), Fyhn et al. (2021), Gaina et al. (2017), Gregersen et al. (2019), Håkansson and Pedersen (2015), Hopper et al. (2014); Japsen et al. (2021a), Nøttvedt et al. (2008), Oakey and Chalmers (2012), Olaussen et al. (2018), Piepjohn et al. (2016); Péron-Pinvidic et al. (2017) and Thorsteinsson and Tozer (1970). (For interpretation of the references to colour in this figure legend, the reader is referred to the web version of this article.)

Baffin Bay and in various continental areas in mid-Paleocene–Eocene times. We here use the term the Eurekan Orogeny to represent the areas and times at which the northward movement of Greenland relative to North America caused deformations in the High Arctic during sea-floor Phases 1 and 2, corresponding to Eurekan Stages 1 and 2 (cf. Gion et al., 2017). The Orogeny is named after Eureka Sound that separates Ellesmere and Axel Heiberg islands. See further discussion in Section 2.

Uplift and erosion near the Cretaceous–Paleogene boundary (Atkinson, 1963; Ricketts, 1994; Arne et al., 1998, 2002; Knudsen et al., 2017; Japsen et al., 2021a) and the Eocene–Oligocene boundary (Blythe and Kleinspehn, 1998; Green and Duddy, 2010; Japsen et al., 2006, 2021b; Dörr et al., 2019) has been reported from many regions in the High Arctic. We therefore combine new and published observations of exhumation from disparate parts of the High Arctic to investigate these episodes in a regional perspective, an approach not previously attempted. We do so by combining (1) new and published low-temperature thermochronology data (apatite fission-track analysis, AFTA, and vitrinite reflectance, VR, data; see Section 3) with (2) stratigraphic information in the context of (3) the plate-tectonic changes in the region.

We present new AFTA and VR data from outcrop and borehole samples from Svalbard, integrate new AFTA and VR data from the Wandel Sea Basin (north of 80°N, east of 40°W) of eastern North Greenland with previously published results and review published thermochronological studies from the Canadian High Arctic, the Lomonosov Ridge and the Barents Sea. We synthesise the data to shed light on the thermal and tectonic history of these regions across the High Arctic, both prior to, during and after the Eurekan Orogeny.

2. The Paleogene plate-tectonic framework

2.1. Slow intra-continental extension (Late Cretaceous – mid-Paleocene)

During the Late Cretaceous, the landmass that now forms Greenland, North America and Eurasia were all parts of the super-

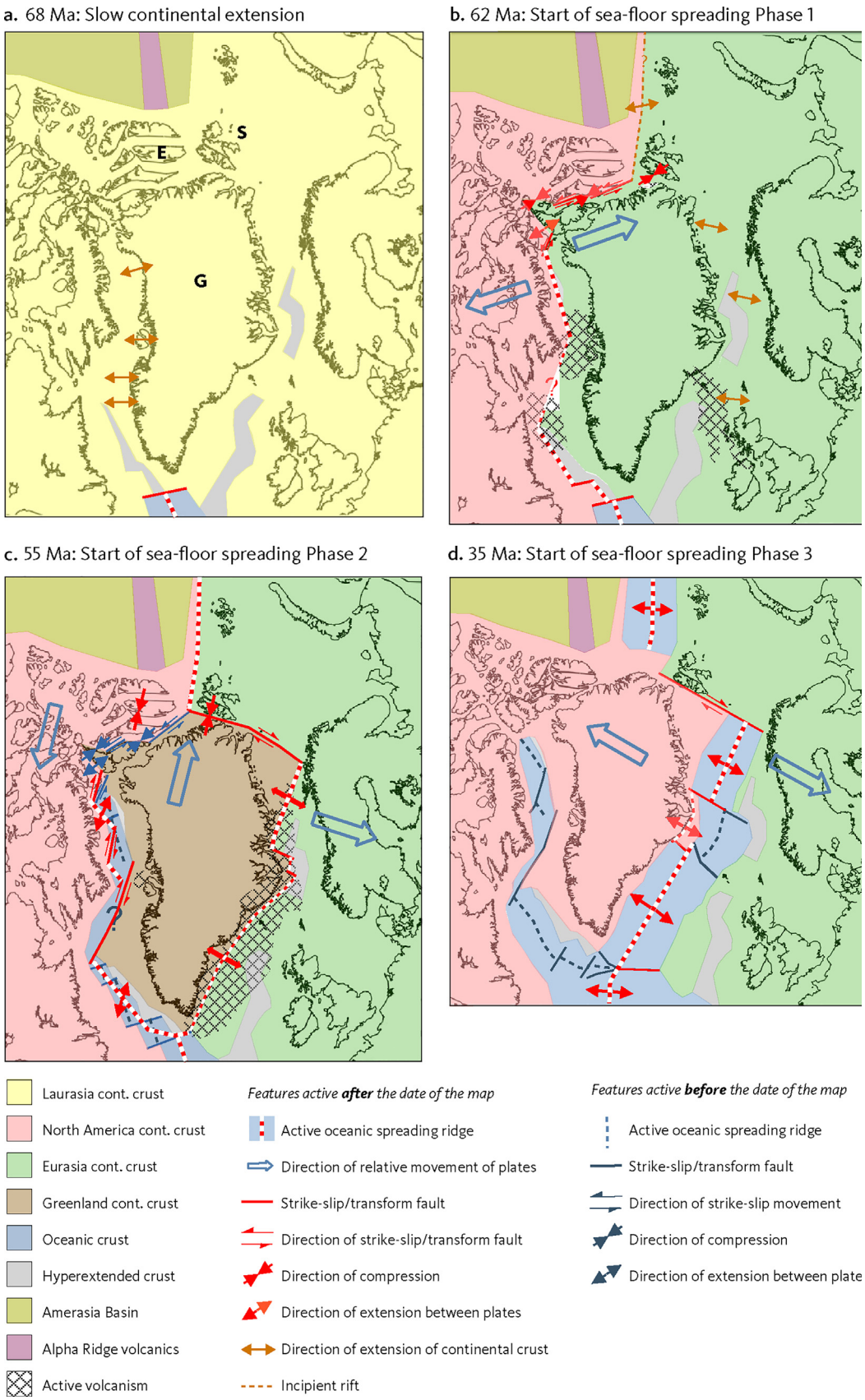
a. 68 Ma: Slow continental extension
S
E
G
b. 62 Ma: Start of sea-floor spreading Phase 1
c. 55 Ma: Start of sea-floor spreading Phase 2
d. 35 Ma: Start of sea-floor spreading Phase 3
Laurasia cont. crust
North America cont. crust
Eurasia cont. crust
Greenland cont. crust
Oceanic crust
Hyperextended crust
Amerasia Basin
Alpha Ridge volcanics
Active volcanism
Features active after the date of the map
Active oceanic spreading ridge
Direction of relative movement of plates
Strike-slip/transform fault
Direction of strike-slip/transform fault
Direction of compression
Direction of extension between plates
Direction of extension of continental crust
Incipient rift
Features active before the date of the map
Active oceanic spreading ridge
Strike-slip/transform fault
Direction of strike-slip movement
Direction of compression
Direction of extension between plate

continent Laurasia. Extensional sedimentary basins had formed during the Mesozoic around Greenland. In places, both east and west of Greenland, the extension had been sufficient to have unroofed the mantle (Figs. 1, 2a; Chian and Louden, 1994; Chalmers and Laursen, 1995; Hopper et al., 2014; Gregersen et al., 2019; Fyhn et al.; 2021 and papers in Péron-Pinvidic et al.; 2017).

Subsidence within some of these sedimentary basins was interrupted in the latest Cretaceous by uplift and erosion; e.g. the North American Arctic and the Barents Shelf (Ricketts, 1994; Arne et al.,1998; 2002). Maastrichtian and base-Paleocene unconformities occur in the Canadian High Arctic, on Svalbard and on– and offshore East and West Greenland (Atkinson, 1963; Embry et al., 2018; Japsen et al., 2005; Dallmann, 2015; Bjerager et al., 2020; Fyhn et al., 2021).

2.2. Sea-floor spreading Phase 1 (late Paleocene): Eurekan Stage 1

Magmatic sea-floor spreading began in Labrador Sea and Baffin Bay at 62.5 Ma (early magnetochron C27N; mid-Paleocene; paleomagnetic timescale from Ogg, 2020; Chalmers and Laursen, 1995). This was coeval with the commencement of high-temperature picritic volcanism on– and offshore West Greenland (Pedersen et al., 2017; Riisager et al., 2003; Larsen and Williamson, 2020). The volcanism is thought to be the surface manifestation of the impact of the Iceland Plume on the base of the lithosphere (Gill et al., 1992; Chalmers et al., 1995; Graham et al., 1998; Dam et al., 1998).

The movement of Greenland relative to North America during sea-floor spreading Phase 1 formed an extensional plate boundary in the Labrador Sea and most of Baffin Bay and Greenland moved nearly 180 km north-east relative to the North American plate (Oakey and Chalmers, 2012; Figs. 2a,b). Sea-floor spreading in the Paleocene did not, however, extend north of present-day northern Baffin Bay, despite the Euler Pole of the movement of Greenland-Eurasia relative to North America during this phase being nearly on the opposite side of the globe (Roest and Srivastava, 1989; Oakey and Chalmers, 2012). This relative movement must have been resolved as some form of transcurrent movement and local compression to the north of Greenland (Figs. 2b,c).

Since Wegener (1912), many authors continue to propose that the movement of the Greenland plate relative to the Canadian Archipelago took place along a single major fault through the Nares Strait, the so-called Wegener Fault (Piepjohn et al., 2016; von Gosen et al., 2019 and references therein). For example, Wilson (1965) cited it as a major transform fault. Other authors have shown that there can be no major transcurrent fault in southwest Nares Strait (Harrison, 2004; Oakey and Damaske, 2006; Pulvertaft and Dawes, 2011; Oakey and Chalmers, 2013). The evidence is too complex to discuss here, but we conclude that there was no single Paleocene "boundary" between Greenland and North American "plates" in the Canadian Archipelago. Instead, the relative movement was distributed across minor extension and an intra-continental transcurrent complex >500 km across on Ellesmere Island, including transpression and local overthrusting on step-overs between strike-slip faults (Figs. 2b,c; Ricketts, 1994; Harrison, 2004, 2008; Oakey and Chalmers, 2012; Embry and Beauchamp, 2019).

Paleocene compression due to the movement of Greenland resulted in exhumation focused along major fault zones in the eastern Sverdrup Basin (Ellesmere and Axel Heiberg islands) leading to high supply of siliciclastic sediment to the adjacent, subsiding areas (Ricketts, 1994; Arne et al., 1998; 2002; Embry and Beauchamp, 2019). A foredeep-like basin thus developed in the eastern Sverdrup Basin during the deposition of the transgressive sandstones of the upper Expedition Formation after c. 62 Ma (Embry et al., 2018; Embry and Beauchamp, 2019). However, Oakey and Chalmers (2012) suggested that the basin formed by extension as parts of eastern Ellesmere Island moved NE relative to Axel Heiberg Island.

Compression causing inversion of fault zones occurred during the mid-Paleocene in the Wandel Sea Basin in NE Greenland (Japsen et al., 2021a; Figs. 2b,c), where heavily deformed Upper Cretaceous and older rocks occur within the major fault zones (Fig. 4a; Harder Fjord Fault Zone, Kap Cannon Fault Zone, Trolle Land Fault Zone; Dawes and Soper, 1973; Håkansson and Pedersen, 1982, 2015; von Gosen and Piepjohn, 2003; Svennevig et al., 2016; Pedersen et al., 2018). Deposition of the fine-grained sandstones, siltstones and coal of the upper Paleocene – middle Eocene Thyra Ø Formation (Fig. 3) was broadly contemporaneous with the inversion of the fault zones (Japsen et al., 2021a).

During the late Paleocene, Greenland moved directly towards Svalbard, which was then still part of the same plate as Greenland (Figs. 2b,c). This movement appears to have led to creation of the West Spitsbergen Fold Belt, as it was formed by E–W- to ENE–WSW-oriented compression (Manby and Lyberis, 1996; Bergh et al., 1997), not by transpression as has been suggested by many authors (e.g., Harland, 1969; Lowell, 1972; Håkansson and Stemmerik, 1989). The shallow-water marine Central Tertiary Basin on Svalbard began to subside in the mid-Paleocene, coeval with the onset of subsidence in the Wandel Sea Basin. Radioisotopic dating of bentonites close to its basal unconformity (below the transgressive sandstones and coal of the Firkanten Fm; Fig. 3) show that the subsidence began around 61.8 Ma, coeval with the start of sea-floor spreading west of Greenland, thus signaling the initiation of compression along the northern Greenland margin (Jones et al., 2017). These observations suggest that the Central Tertiary Basin is a foreland basin in front of the developing West Spitsbergen Fold Belt as has previously been suggested (Dallmann, 2015).

We refer to the deformations that affected the High Arctic during sea-floor spreading Phase 1 as Stage 1 of the Eurekan Orogeny.

2.3. Sea-floor spreading Phase 2 (Eocene): Eurekan Stage 2

Sea-floor spreading, accompanied by widespread sub-aerial volcanism (Horni et al., 2017), began between Greenland and Eurasia in the earliest Eocene (C24, c. 55 Ma; Gaina et al, 2017), resulting in Greenland moving as a plate separate from both North America and Eurasia. North of Greenland there was, however, no clear

Fig. 2. Plate reconstructions around the North-East Atlantic from the Maastrichtian to the end of the Eocene. After Mesozoic extension east and west of Greenland, sea-floor spreading moved Greenland relative to the North American and Eurasian plates in the Paleogene in three phases. (a) 68 Ma, late Maastrichtian: There has been extension between Greenland and Canada and between Greenland and Eurasia. Hyper-extension in some areas has unroofed the mantle. (b) 62 Ma, mid-Paleocene: Onset of Phase 1 of sea-floor spreading west of Greenland while Greenland and Eurasia moved together resulting in Greenland moving 180 km north-east relative to the North American Plate. This movement led to Stage 1 of the Eurekan Orogeny in the High Arctic. (c) 55 Ma, earliest Eocene: Onset of Phase 2 of sea-floor spreading east of Greenland that, together with continued sea-floor spreading west of Greenland, caused Greenland to move north relative to the Arctic Islands where the resulting compression caused Stage 2 of the Eurekan Orogeny. (d) 35 Ma, late Eocene: Just before the onset of Phase 3 of sea-floor spreading (33 Ma) when Greenland became attached to North America as spreading west of Greenland ceased, a major change in the North-East Atlantic spreading system took place and the Eurekan Orogeny ended. The movements shown were generated by the G-Plates software using the Matthews et al. (2016) reconstructed coastline locations within that software. Geological details were added from Oakey and Chalmers (2012) and Gregersen et al. (2019) for areas between Canada and Greenland and within Ellesmere Island, Gaina et al. (2017) and Stoker et al. (2017) for the area east of Greenland. cont.: continental. E: Ellesmere Island. G: Greenland. S: Svalbard.

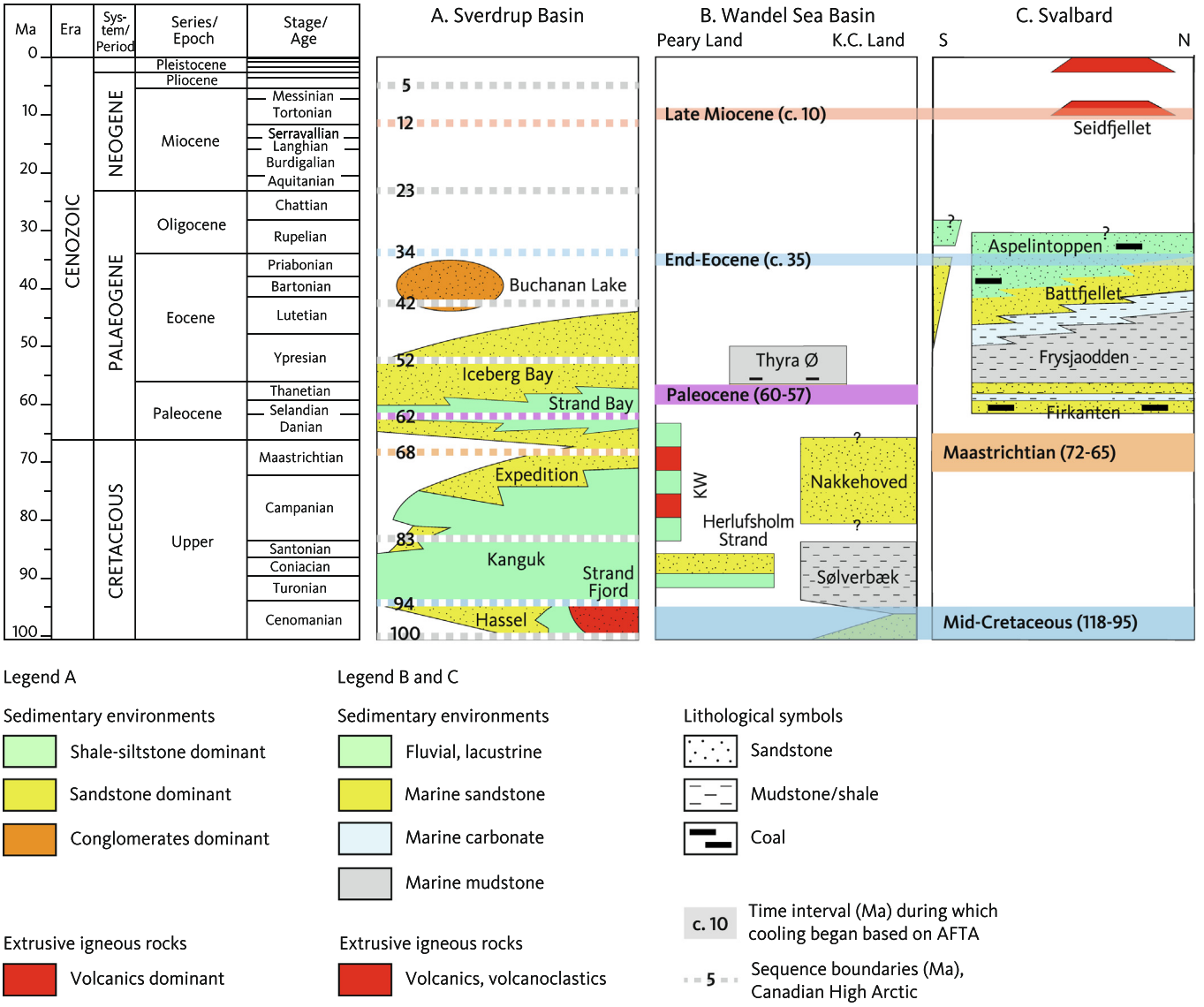

Fig. 3. Late Cretaceous – Cenozoic stratigraphic columns. (a) The Sverdrup Basin. (b) the Wandel Sea Basin (WSB). (c) Svalbard with selected formation names. The stratigraphy is compared with the timing of the cooling episodes from AFTA in the WSB and Svalbard (horizontal bars; Fig. 7). The vertical extent of the horizontal, colored bars indicates the uncertainty in the onset timing of the cooling episode, although the full uncertainty in the onset of the mid-Cretaceous episode (118–95 Ma) is not shown. The stratigraphy of the Sverdrup Basin is compared with large-magnitude sequence boundaries for the Canadian High Arctic (including the Beaufort-Mackenzie Delta) that are interpreted to be the result of tectonism (dashed bars; Embry et al., 2018). Sequence boundaries that correspond to the onset of cooling events from AFTA for the WSB and Svalbard (this study) are shown in the corresponding colors, whereas additional sequence boundaries are marked in grey. Note that the mid-Paleocene unconformity, dated at 62 Ma in the Canadian High Arctic, is not resolved in the stratigraphy shown in column a. The stratigraphic ages of the Eocene sediments on Svalbard (column c) are not well defined (Helland-Hansen and Grundvåg, 2020), so we suggest that the exhumation that began at c. 35 Ma defines a Priabonian age for the youngest Paleogene sediments on Svalbard. The Paleogene sediments to the left in column c represent the deposits in Forlandsundet. Simplified representation of the mixed volcanic, volcano-clastic and lacustrine deposits of the Kap Washington Group (KW) in column b. Sverdrup Basin stratigraphy from Embry and Beauchamp (2019). WSB stratigraphy compiled by Japsen et al. (2021a) based on Bjerager et al. (2019), Gautier et al. (2011), Håkansson and Pedersen, (2015), Hopper et al. (2014), Hovikoski et al. (2018), Ineson et al. (2020), Lyck and Stemmerik (2000), Piasecki et al. (2018), Stemmerik et al. (1998), Svennevig et al. (2018) and Tegner et al. (2011). Svalbard stratigraphy based on the compilation of Dallmann (2015) with modifications from Abay et al. (2017) and Jones et al. (2017). K.C. Land: Kronprins Christian Land.

boundary between the Greenland and North American plates, where deformation was intra-continental, resulting in complex overthrusting. The 3-plate movements resulted in the movement of Greenland relative to North America changed from north-east in the Paleocene to north in the Eocene (Figs. 2b,c). The new spreading center in the Labrador Sea and Baffin Bay cut across the Paleocene oceanic crust with an Euler Pole to the west of and much closer to Greenland than the Euler pole in the Paleocene (Oakey and Chalmers, 2012).

The northward movement of Greenland relative to the Canadian Arctic islands during the Eocene resulted in compression and southwards-verging overthrusting on Ellesmere Island; (Fig. 1; Harrison, 2008; Piepjohn et al., 2015; Gion et al, 2017). Some of the strike-slip movements postulated to have taken place during Eurekan Orogeny Stage 1 during the late Paleocene may have been obscured by this thrusting. Thus, there was no clear plate boundary between the Greenland and North American plates in this area, just a major area of intra-continental compression and deformation.

Sea-floor spreading in the Eurasia Basin north-east of Greenland, combined with the start of sea-floor spreading in the North-East Atlantic (Fig. 1) formed a major intra-continental transform fault, the De Geer Line (Figs. 2c,d), between Greenland on one side and Svalbard and the Barents Shelf on the other. Many authors have argued that transpression during this movement was the pri-

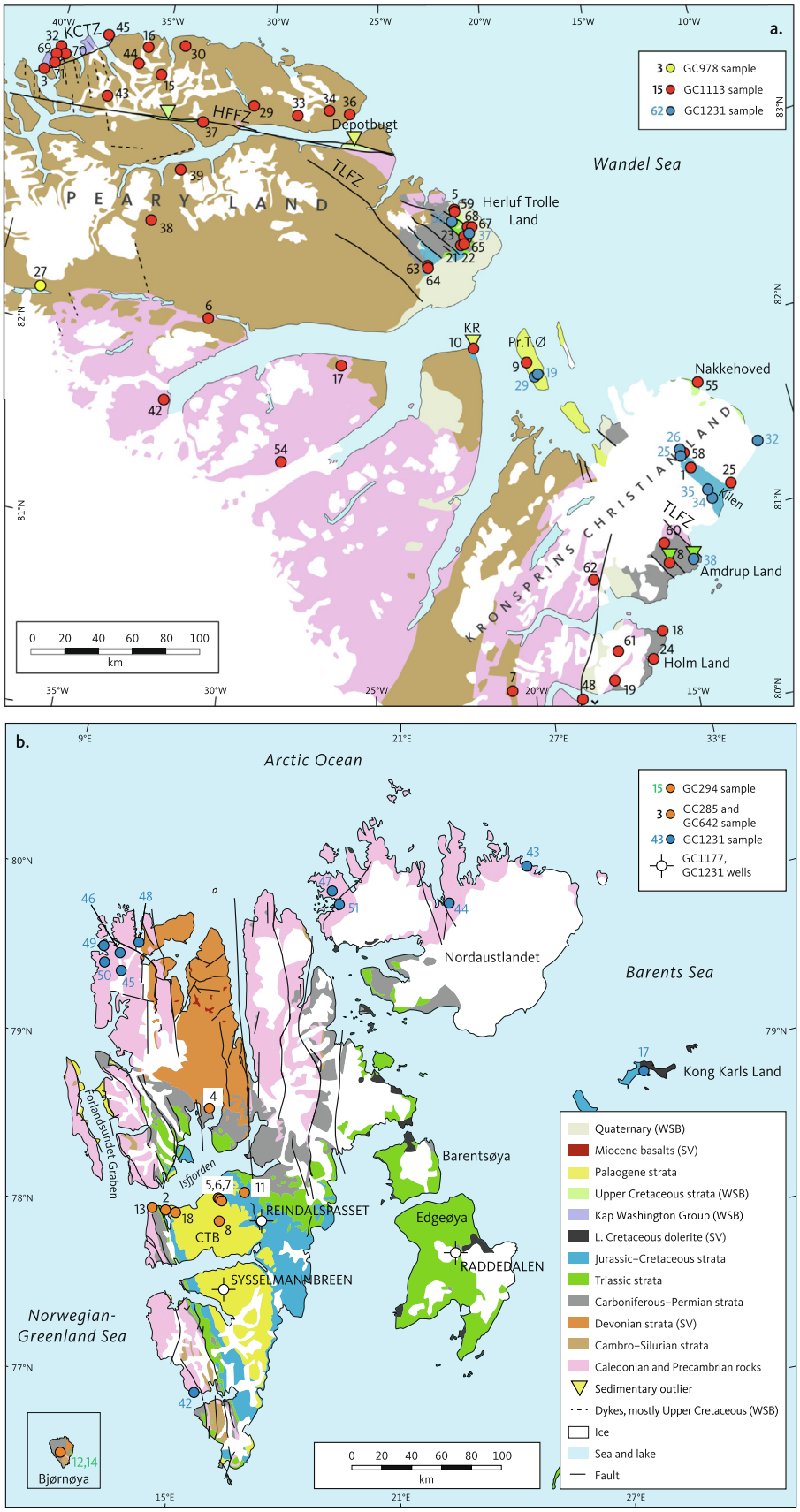

Fig. 4. Geology and location of AFTA samples. (a) The Wandel Sea Basin. Triangles indicate sedimentary outliers and point to their location. (b) Svalbard Archipelago. CTB: Central Tertiary Basin. HFFZ: Harder Fjord Fault Zone. KCTZ: Kap Canon Thrust Zone. KR: Kap Rigsdagen. Pr. T. Ø: Prinsesse Thyra Ø. TLFZ: Trolle Land Fault Zone. Map in (a) compiled by Japsen et al. (2021a) based on Escher and Pulvertaft (1995) with modifications after Croxton et al. (1980), Hovikoski et al. (2018); Piasecki et al. (2018). Map in (b) from Dörr et al. (2018) redrawn after Dallmann et al. (2002). Geology legend common for both maps (SV: Svalbard only; WSB: Wandel Sea Basin only). Map locations in Fig. 1.

mary cause of the West Spitsbergen Fold Belt (Harland, 1969; Lowell, 1972; Håkansson and Stemmerik, 1989). However, Manby and Lyberis (1996) and Bergh et al. (1997) showed that the movement during this phase was relatively minor, dextral transpression that overprinted the earlier SW–NE compression, accompanied by NE–SW extension that presumably led to the deepening of the southwestern part of the Central Tertiary Basin in the Eocene (Dörr et al. 2018).

We refer to the deformations that affected the High Arctic during sea-floor spreading Phase 2 as Stage 2 of the Eurekan Orogeny.

2.4. Sea-floor spreading Phase 3 (post end-Eocene): Post-Eurekan

Sea-floor spreading both east and west of Greenland slowed after C21 (c. 43 Ma, mid-Eocene; Srivastava and Keen, 1995; Gaina et al., 2017). West of Greenland, sea-floor spreading ceased entirely after C13 (33 Ma, earliest Oligocene; Srivastava, 1978). Thereafter, Greenland moved together with the North American Plate and the Eurekan Orogeny ceased (Fig. 2d; Tessensohn and Piepjohn, 2000; Oakey and Chalmers, 2012; Piepjohn et al., 2016). East of Greenland, sea-floor spreading was very slow between 34 and 27 Ma (Gaina et al. 2017).

Regional exhumation that began at both the Eocene–Oligocene transition and in the late Miocene has been reported for the Sverdrup Basin, the Wandel Sea Basin, North-East Greenland (70–80°N), Svalbard and the Barents Sea (Blythe and Kleinspehn, 1998; Green and Duddy, 2010; Dörr et al., 2019; Japsen et al., 2021a, b). We discuss this in more detail in Section 5.4.

3. Thermal history reconstruction based on AFTA and VR data from the Wandel Sea Basin and Svalbard

3.1. AFTA and VR

Paleothermal methods such as AFTA and VR allow determination of events in which rocks cooled from higher temperatures (e.g. Green and Duddy, 2012). In many situations the dominant cause of cooling is exhumation, i.e. removal of overburden resulting in rocks being raised from depth to shallower levels (Green et al., 2013, 2018a). Thus, these methods allow determination of former burial depths and therefore the amount of section that was once present but is no longer preserved (missing section). AFTA also allows determination of the timing of the onset of cooling/exhumation. Integrating such information with preserved geological evidence allows a more complete reconstruction of past events and can define major periods of tectonism which may not be obvious from the preserved geological record alone (Japsen et al., 2006; 2016; Green et al., 2022a, b).

AFTA relies on analysis of radiation damage trails (fission tracks) in apatite grains, which may be either accessory (in crystalline rocks) or detrital (in sedimentary rocks). Tracks are generated continuously by spontaneous fission of ^{235}U atoms, present at impurity levels within the apatite lattice. Once formed, tracks shorten at a rate which depends on temperature due to repair of the radiation damage. As a result, the distribution of track lengths in an apatite today records the variation in temperature with time below c. 110–130°C (depending on apatite composition). The number of tracks per unit area of a polished grain surface (track density) depends on the uranium content of the apatite, the time over which tracks have accumulated and the distribution of track lengths in the sample. Measuring the track density and the uranium content allows determination of a 'fission-track age' which, in the absence of other factors, would represent the time over which tracks have accumulated. However, because tracks have different lengths as a result of the thermal history, a fission track age

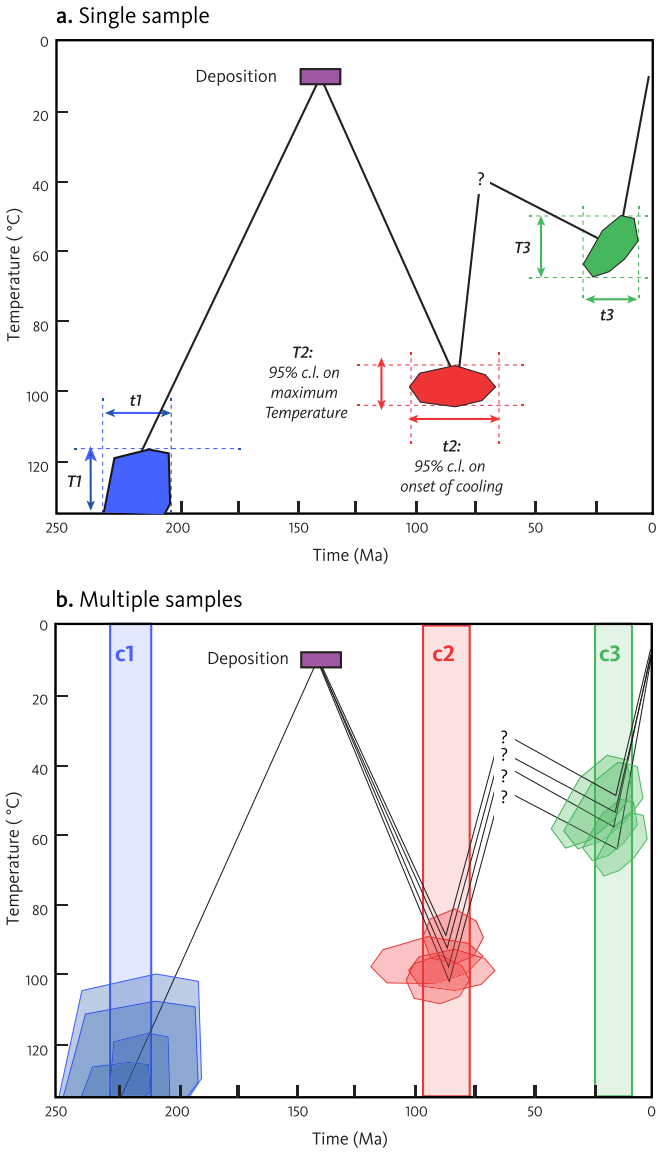

Fig. 5. Thermal history interpretation of AFTA data in a sedimentary rock. (a) Data from a single sample are interpreted in terms of up to three episodes of cooling from elevated paleotemperatures ("paleothermal episodes"). The first cooling event represents cooling of apatite grains from paleotemperature interval **T1** in the time interval **t1** in sediment source terrains (T1 is a minimum estimate, representing the onset of track retention). This cooling and exhumation resulted in the apatite grains being exposed on the surface prior to deposition in the host sediment. Following deposition, the sample was heated to **T2** prior to cooling which began in the interval **t2**. After this cooling episode the sample was subsequently reheated to **T3**, from which cooling began in the interval **t3**. Coloured polygons represent 95% confidence regions on T1, T2, T3, t1, t2, t3. Note that the history between the two cooling episodes cannot be constrained (Green and Duddy, 2020). (b) Results from multiple samples can be combined to estimate the onset of cooling episode consistent with all available constraints, c1, c2, c3. These are interpreted as representing the best available estimate of the onset of regional cooling episodes. (For interpretation of the references to colour in this figure legend, the reader is referred to the web version of this article.)

rarely represents the timing of a specific event and must be assessed together with the distribution of track lengths in order to obtain rigorous thermal history constraints. Analysis of the number of tracks and their lengths allows determination of major episodes of cooling in the range below c. 110°C (Fig. 5a). It is important to note that AFTA cannot define the entire thermal history below 110°C, as the data are dominated by major cooling episodes, which mask the earlier history (see Green and Duddy, 2012, 2020).

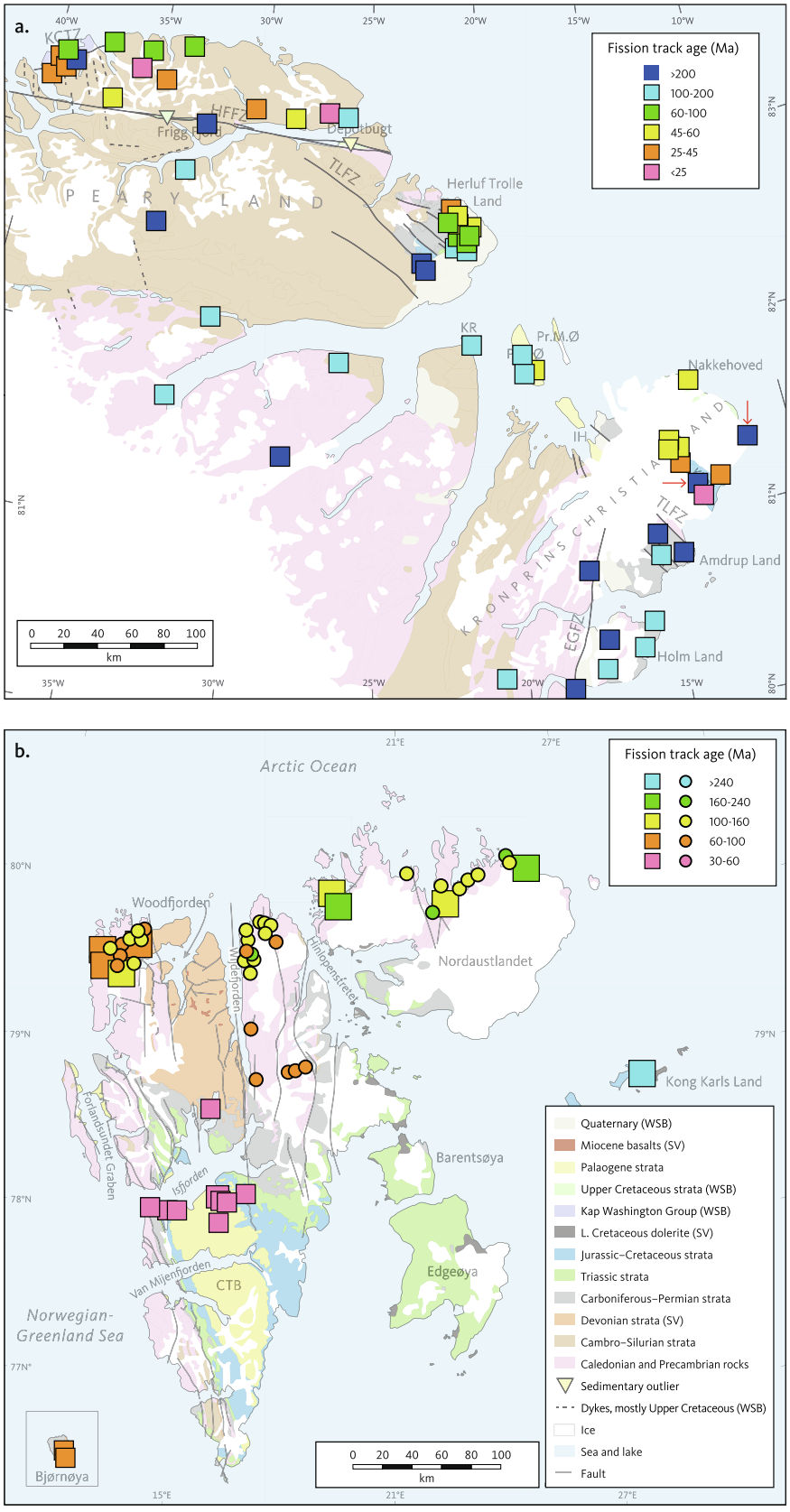

Fig. 6. Apatite fission-track ages measured in samples from outcrop locations (squares). (a) The Wandel Sea Basin (WSB). (b) Svalbard (SV), together with data from Dörr et al. (2012, 2018) (circles). Fission-track ages for samples GC1231-32 and −35 (red arrows, Fig. a), from locations in Kronprins Christian Land, gave much older than values in nearby samples. These anomalies may represent sample mis-identification or mistaken sample locations. These samples are not illustrated in the Paleocene paleotemperature map in Fig. 8a. (For interpretation of the references to colour in this figure legend, the reader is referred to the web version of this article.)

VR is based on the increase in reflectivity of vitrinite (a major constituent of coal) with temperature. The mean VR value of a number of vitrinite fragments in a carbon-rich mudstone or coaly matter in sandstones is dominated by the maximum temperature experienced by the host unit. The kinetics of AFTA and VR are similar (Green and Duddy, 2012) and use of the methods in tandem provides mutual confirmation of the thermal history derived from each method in isolation (e.g. Green et al., 2018b).

3.2. AFTA and VR data in this study

In order to understand more fully the processes involved in the disruption of Arctic basins, we obtained AFTA and VR data in samples from the Wandel Sea Basin and Svalbard (Tables S1–S5 in Supplementary Data 1). Details of AFTA and VR data, together with analytical details, thermal history interpretation and technical background, are provided in Supplementary Data 2 (Green, 2020). A file with sample coordinates in kmz format for GoogleEarth is provided in Supplementary Data 3 (location of AFTA samples in Fig. 4). These data have been integrated with published data from Arctic Canada (Arne et al., 1998, 2002; Vamvaka et al., 2019).

From the Wandel Sea Basin, we obtained AFTA data in 58 outcrop samples varying in age from Precambrian to Paleocene; data in 13 samples were generated for this study (prefix GC1231, samples GC1113-69, −70, −71), while data in 45 samples (prefix GC978 and other samples with prefix GC1113) were presented by Japsen et al. (2021a).

From Svalbard, we obtained AFTA data in 22 outcrop samples varying in age from Precambrian to Paleocene. Data in 12 samples were generated for this study (prefix GC1231), while data in the remaining outcrop samples were derived from previous (unpublished) studies. AFTA data were also obtained in 12 samples of Carboniferous to Eocene age from three Svalbard boreholes from depths down to 2.3 km; the Sysselmannbreen (Johannessen et al., 2011), Reindalspasset (well 7816/12–1) and Radderdalen boreholes (prefix GC1177 for the first of these boreholes and prefix GC1231 for the latter two). Equinor provided outcrop and borehole samples from Svalbard (prefix GC1177, GC1231) and GEUS provided outcrop samples from North Greenland (prefix GC1231). It is important to note that the coverage of AFTA samples across Svalbard is sparse and that it does not include the West Spitsbergen Fold Belt.

We also obtained new VR data in three samples from outcrops in Wandel Sea Basin, while published VR data from that region were reviewed by Japsen et al. (2021a). The Svalbard dataset includes VR data in 8 outcrop samples and 11 borehole samples together with legacy VR data in the boreholes.

Apatite fission-track ages in all but one outcrop sample across the Wandel Sea Basin and Svalbard are less than 300 Ma and are mainly less than 200 Ma (Fig. 6). In areas dominated by Precambrian rocks this emphasizes that thermal histories are dominated by the post-Paleozoic development. In the Wandel Sea Basin, youngest ages are focused along the north and northeast coasts with older ages confined mainly to the interior. This suggests that the younger ages may reflect processes related to the development of the plate boundary. In contrast, youngest ages in Svalbard are focused along Isfjorden, mainly within the Central Tertiary Basin.

VR values from outcrops across the Wandel Sea Basin vary across the region (figure 12 of Japsen et al. 2021a). With a few exceptions, the variation in mean VR values across the region can be divided into three categories: 1) 0.4%–0.6% in samples of Jurassic–Paleocene depositional age in inland regions, 2) 1%–3% in samples of Jurassic–Cretaceous depositional age mainly within fault zones of the Wandel Sea Basin, and 3) extreme values up to 10% in samples of Late Cretaceous age from Nakkehoved at the northern tip of Kronprins Christian Land (Japsen et al., 2021a). VR values vary across Svalbard from 0.36% in Barremian sediments on the eastern islands of Kong Karls Land to 0.45%–0.73% for Lower Cretaceous and Paleogene sediments in and adjacent to the Central Tertiary Basin. Values for Carboniferous sediments reach 2.04% northwest of Isfjorden.

3.3. Thermal history constraints from AFTA and VR data

Thermal history constraints obtained from the AFTA data in each sample are summarized in Table S5 in Supplementary Data 1. These take the form of estimates of the time at which cooling began and the paleotemperature from which the sample cooled, in up to three episodes (Fig. 5a). The quoted intervals represent 95% confidence limits (i.e. akin to 2σ uncertainties) in each parameter. The principles involved in extracting quantitative thermal history constraints from AFTA and VR data are outlined in Appendix C of Supplementary Data 2. Note that some values have changed from those reported in Supplementary Data 2, as a result of a reassessment of the entire dataset. For sandstone samples in which the apatites were not totally annealed after deposition, these constraints include both pre-depositional and post-depositional cooling episodes. In discussing implications for regional tectonics, we focus on post-depositional episodes, and constraints on pre-depositional cooling of provenance terrains are not used to define timing of regional episodes. In the following, we use the term 'paleothermal episode' to refer to a time when samples were hotter than they are now, whereas 'cooling episode' refers specifically to a time in which samples began to cool from elevated paleotemperatures.

If we assume (1) that the results represent the effects of regional processes which involved synchronous cooling over wide areas, and (2) that cooling episodes in adjacent samples that cooled from similar paleotemperatures within a common time interval represent the same event, we can synthesise results from all samples to define the timing of the major cooling events that have affected each region (vertical bands in Fig. 5b). We emphasise that these intervals define the time at which cooling in each episode began, but we do not suggest that cooling was restricted to within these intervals.

Comparison of timing constraints on the regional cooling episodes defined from AFTA data in outcrop and borehole samples from the Wandel Sea Basin and Svalbard show that six regional episodes are required to explain all results, while one episode is identified only in the Wandel Sea Basin and one episode only in Svalbard (Table 1; Fig. 7a). The onsets of cooling in each of these episodes are consistent with those defined by Japsen et al. (2021a) for the Wandel Sea Basin, with two exceptions: The Maastrichtian episode, which is defined only in new data from Svalbard, and the earliest of these episodes, which was previously identified as beginning in the early Permian, has been revised as beginning in the mid-Carboniferous.

Table 1
Intervals defining the onset of episodes of cooling based on AFTA data in all samples from the Wandel Sea Basin and Svalbard.

Onset of cooling (Ma)	Onset of cooling (chronostratigraphy)
326–320	Mid-Carboniferous
234–229	Late Triassic
173–150	Jurassic
118–95	Mid-Cretaceous
72–65	Maastrichtian†
60–57	Paleocene‡
c. 35	End-Eocene
c. 10	Late Miocene

† Svalbard only.
‡ Wandel Sea Basin only.

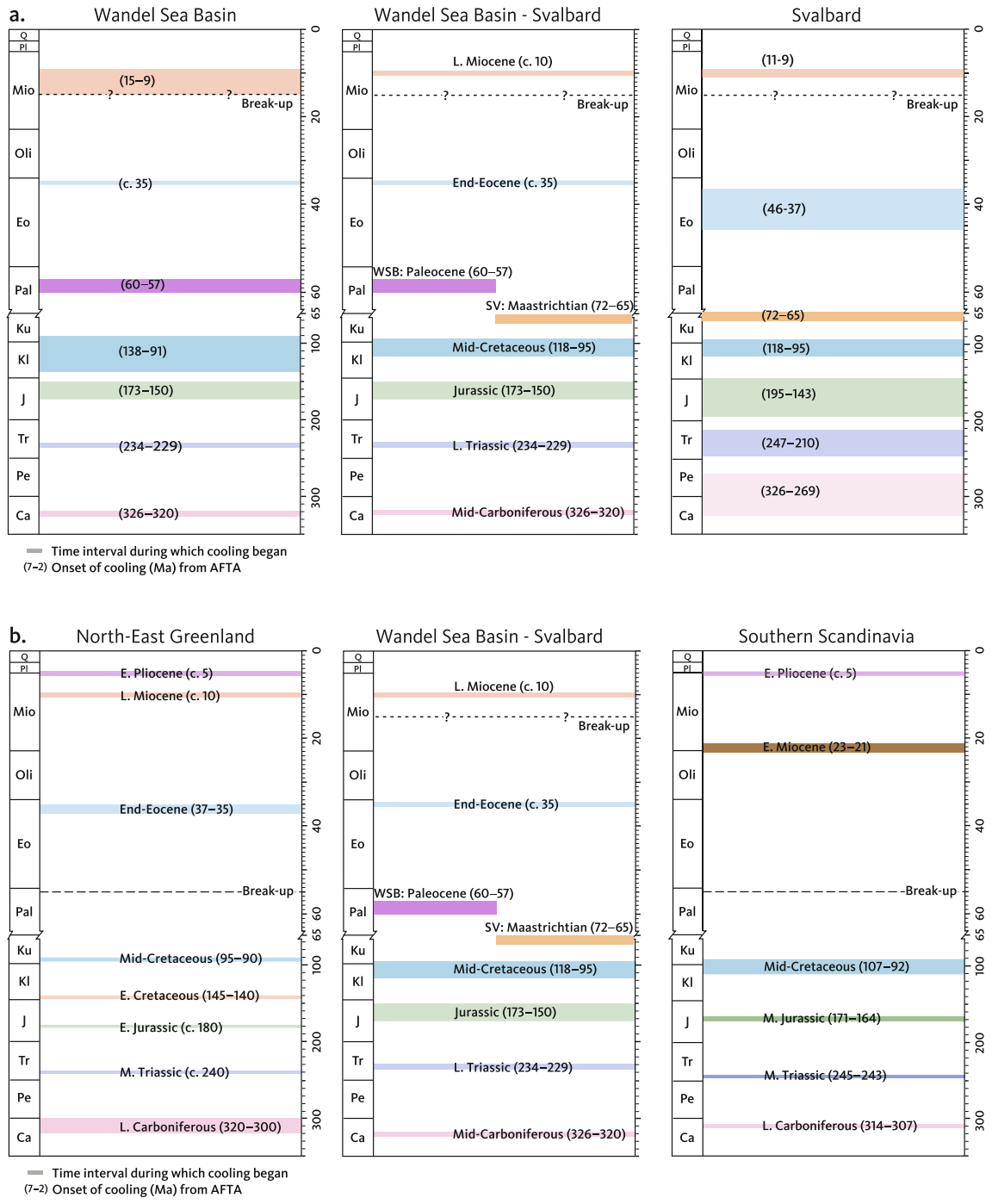

Fig. 7. Onset of cooling episodes defined from AFTA. (a; Table 1) Left: Wandel Sea Basin (WSB). Centre: Overlap in the timing for the episodes defined for the WSB and Svalbard. Right: Svalbard. Six regional cooling episodes are required to explain all results, while one episode is identified only in the WSB and one episode only in Svalbard. (b) Comparison of the timing of regional, post-Devonian episodes of uplift and erosion estimated from AFTA data. Left: North-East Greenland (70–80°N; Japsen et al., 2021b). Centre: WSB and Svalbard (Table 1). Right: Scandinavia and Finland (Green et al., 2022b). Break-up in the North-East Atlantic, took place in the earliest Eocene (c. 55 Ma), whereas sea-floor spreading in the Fram Strait between North Greenland and Svalbard began in the Miocene (Engen et al., 2008; Knies and Gaina, 2008; Gaina et al., 2017; Dumais et al., 2021). L: Late. E: Early. M: Mid. C: Carboniferous. Pe: Permian. Tr: Triassic. J: Jurassic. Kl: Lower Cretaceous. Ku: Upper Cretaceous. Pal: Paleocene. Eo: Eocene. Oli: Oligocene. Mio: Miocene. Pl: Pliocene. Q: Quaternary. (For interpretation of the references to colour in this figure legend, the reader is referred to the web version of this article.)

3.3.1. Comparison with regional data

Late Carboniferous, Middle Triassic and mid-Jurassic exhumation episodes affected Scandinavia and North-East Greenland at about the same time (beginning at c. 310, 245 and 175 Ma), and these episodes were interpreted as representing epeirogenic uplifts accompanying fragmentation of Pangea (Japsen et al., 2016; Green et al., 2022b). However, the episodes of exhumation at about these times that affected North Greenland and Svalbard show some variation in timing compared to those further south (Fig. 7b). Evidence from the stratigraphic record indicate that these episodes most likely began at c. 325, 235 and 175 Ma (Dallmann, 2015; Japsen et al., 2021a). The mid-Jurassic episode thus appears to have affected the entire region from Svalbard to southern Sweden at about the same time, whereas there are time lags for the two ear-

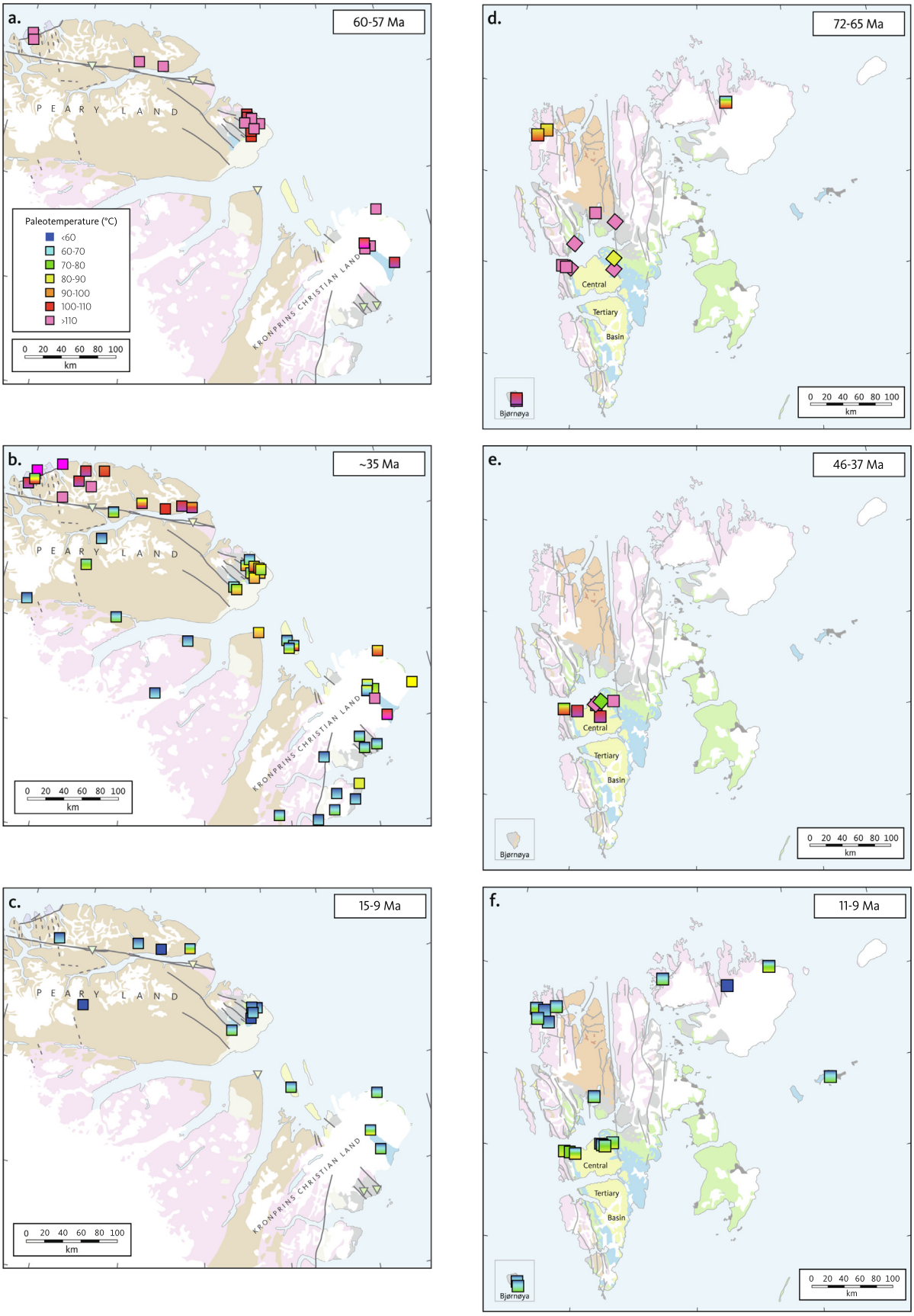

Fig. 8. Paleotemperatures derived from AFTA and VR data in outcrop samples (Table S5 in Supplementary Data online). Assignment to regional cooling episodes according to Fig. 7a. (a) Wandel Sea Basin (WSB), Paleocene. (b) WSB, end-Eocene. (c) WSB, late Miocene. (d) Svalbard, Maastrichtian. (e) Svalbard, end-Eocene. (f) Svalbard, late Miocene. Squares: Values from AFTA. Diamonds: Values from VR data from Svalbard have been attributed to one of the regional cooling episodes by comparison with AFTA data in adjacent samples. Sample numbers and place names in Fig. 4. Geology legend in Fig. 6.

lier episodes across the region. The mid-Carboniferous episode defined in this study correlates with a pronounced unconformity in Svalbard and North Greenland, reflecting Serpukhovian uplift of the northern margin of Pangea (Stemmerik and Worsley, 2005), and it therefore seems likely that this episode represents a different process relative to the late Carboniferous episode defined further south. The onset of the mid-Cretaceous episode in this study area correlates closely with episodes in North-East Greenland and southern Scandinavia, indicating that all these results reflect a common episode in the earliest Late Cretaceous, around 95 Ma, affecting a wide region.

We do not discuss these earlier episodes further because we focus on the tectonism associated with continental breakup and sea-floor spreading west and east of Greenland and its relevance to the effects of the Eurekan Orogeny in the High Arctic.

4. Thermo-tectonic events in relation to the Eurekan Orogeny

4.1. The Wandel Sea Basin

Paleocene cooling is localised within the major fault zones of the Wandel Sea Basin and is interpreted as representing exhumation related to inversion of these zones (Fig. 7a, 8a; Table S5 in Supplementary Data 1; Japsen et al., 2021a). Most of the samples defining Paleocene cooling began to retain tracks in this episode and provide minimum limits, typically > 110°C, to the Paleocene paleotemperature.

The timing of Paleocene cooling in the Wandel Sea Basin is based on samples which cooled below a certain limiting paleotemperature at that time, corresponding to the onset of track retention. Cooling from maximum paleotemperatures in these samples may thus have begun earlier, i.e. prior to 60 Ma. Samples that cooled from a finite range of paleotemperatures during this episode began to cool after 69 Ma (Table S.5). Therefore an alternative range for the onset of cooling and exhumation of this episode could be between 69 and 57 Ma, which overlaps with the timing of Maastrichtian cooling in Svalbard (Section 4.2). However, the geographical distributions of the exhumation that occurred around the Maastrichtian–Paleocene boundary in Svalbard and the Wandel Sea Basin are distinctly different (Figs. 8a,d). Whereas Maastrichtian exhumation was widespread on Svalbard (Section 4.2), the exhumation in the Wandel Sea Basin is focused along the major fault zones that were inverted during the late Paleocene Stage 1 of the Eurekan Orogeny. Although the timing constraints allow overlap, based on the different geographical expressions of these events, we conclude that the AFTA data provide evidence for two distinct episodes, regional Maastrichtian exhumation on Svalbard cf. Paleocene inversion of fault zones in the Wandel Sea Basin.

Cooling which began at the end of the Eocene is seen in almost all samples across the Wandel Sea Basin (Fig. 8b). Samples over much of the area cooled from paleotemperatures around 70–90°C at this time, including samples of the Thyra Ø Formation (Fig. 3). These paleotemperatures reflect burial of the Thyra Ø Formation and younger Eocene sediments below a cover of about 2.5 km (assuming a paleogeothermal gradient of 30°C/km and paleosurface temperature of 10°C) which has subsequently been eroded away. However, samples located north of the Harder Fjord Fault Zone, together with some samples from northern Kronprins Christian Land, cooled from paleotemperatures > 100°C at this time. Because these samples began to retain tracks only in this episode, it is therefore possible that they previously also underwent major Paleocene cooling, the effects of which are overprinted by the end-Eocene paleotemperatures.

Late Miocene cooling from paleotemperatures generally around 60°C is recognized along the coast of eastern North Greenland (Fig. 8c). In West and East Greenland, late Miocene cooling reflects uplift and erosion of the continental margin and development of the present-day topography, and we suggest that the late Miocene episode identified in the Wandel Sea Basin shares the same origin (Fig. 7b; Japsen et al., 2006, 2014, 2021b).

Japsen et al. (2021a) compiled existing VR data from sedimentary rocks of the Wandel Sea Basin and discussed the regional variation in relation to the AFTA database then available. VR values define maximum post-depositional paleotemperatures which are consistent with the AFTA data in different paleothermal episodes. In some samples VR data assist in resolving pre-depositional from post-depositional events. The combination of AFTA and VR data is central for resolving the effects of localised Paleocene paleothermal cooling from > 110°C and more regional end-Eocene cooling from 70 to 90°C.

4.2. Svalbard

4.2.1. New data from Svalbard outcrops

Maastrichtian cooling is identified in samples across a wide part of Svalbard, and this cooling episode dominates the AFTA data in samples along Isfjorden with paleotemperatures > 110°C (Fig. 8d; Table S5 in Supplementary Data 1). Maximum paleotemperatures derived from VR data in samples of pre-Cenozoic depositional age around Isfjorden are generally consistent with Maastrichtian paleotemperatures from the AFTA data. Maastrichtian cooling from lower paleotemperatures (80–100°C) is identified in some samples from the northwest of the region. In two samples from Bjørnøya, paleotemperatures in this event are > 105°C. The Maastrichtian cooling corresponds to the Albian – mid-Paleocene hiatus in the Central Tertiary Basin (Fig. 3), and we interpret cooling in this episode as due to exhumation during the interval represented by this hiatus following deeper burial prior to c. 68 Ma.

End-Eocene paleotemperature constraints defined from AFTA are seen only in samples along Isfjorden, with values around 100°C or above (Fig. 8e). No end-Eocene cooling is detected in samples along the northern coast of Svalbard. The end-Eocene cooling corresponds to the late Eocene – Quaternary hiatus in the Central Tertiary Basin, and we interpret cooling in this episode as due to exhumation during the interval represented by this hiatus following deeper burial prior to c. 35 Ma.

Late Miocene cooling is seen in all samples across the region with values in the range 60–80°C (Fig. 8f). Outside the main locus of Maastrichtian and Eocene paleothermal effects, it is possible that paleotemperatures in these events were too low to be resolved from Miocene values. Like the end-Eocene cooling episode, we interpret cooling in this episode as due to exhumation during the late Eocene – Quaternary following deeper burial prior to c. 10 Ma. Late Miocene uplift in northern Svalbard initiated the formation of the present-day elevated landscapes (Dörr et al., 2019).

4.2.2. New data from Svalbard boreholes

The Reindalspasset and Sysselmannbreen boreholes are located at the edge of and within the Central Tertiary Basin, respectively (Fig. 4b). AFTA and VR data in samples from these wells define constraints which are consistent with the three most recent episodes of cooling defined from the full dataset from Svalbard and the Wandel Sea Basin (Maastrichtian, end-Eocene and late Miocene episodes; Figs. 7a, 9b; Table S5 in Supplementary Data 1). For each episode, the paleotemperature constraints for each borehole can be described by linear depth profiles that are sub-parallel to the present-day temperature profile, indicative of heating due to deeper burial.

The Carboniferous to Lower Cretaceous succession in the Reindalspasset borehole began to cool from maximum post-depositional paleotemperatures in the Maastrichtian. Variation of

the Maastrichtian paleotemperatures with depth in this borehole is consistent with a paleogeothermal gradient similar to the present-day value (c. 30°C/km; Fig. 9c), suggesting that heating was due to additional burial by c. 4.3 km of Cretaceous section. Additional burial when cooling began in the end-Eocene and late Miocene episodes is estimated at c. 2.1 km and at c. 1.3 km, respectively (Figs. 9c, 10).

In contrast, the upper Paleocene – lower Eocene succession penetrated by the Sysselmannbreen borehole cooled from maximum post-depositional paleotemperatures in the end-Eocene episode. Paleotemperatures are again consistent with a paleogeothermal gradient similar to today's value (c. 30°C/km; Fig. 9c), indicating that around 2 km of upper Eocene sediments accumulated above the youngest Eocene sediments penetrated by the well (the Aspelintoppen Formation; Fig. 3) prior to the onset of exhumation. The removal of this former cover began during end-Eocene exhumation. The stratigraphic ages of the Eocene sediments on Svalbard are not well defined (Dallmann, 2015; Helland-Hansen and Grundvåg, 2020). So, since exhumation began at c. 35 Ma, the youngest sediments deposited prior to the onset of exhumation must be older than that. Therefore, the youngest Paleogene sediments that accumulated on Svalbard must be of Priabonian age (Fig. 3).

4.2.3. Previous exhumation studies in Svalbard and the Barents Sea

Manum and Throndsen (1977) measured VR in the Paleogene deposits in the Central Tertiary Basin. At the location of the Sysselmannbreen borehole, they estimated the maximum burial depth to be between 3 and 3.5 km for the base of the Paleogene succession, the Firkanten Formation (Fig. 3), which is of mid-Paleocene age (Jones et al., 2017). This is in good agreement with our estimate of 3.2 km (penetrated + removed Paleogene succession = 1.1 + 2.1 km; Fig. 9). Paech and Koch (2001) presented results of an extensive study of coalification in post-Caledonian sediments on Spitsbergen, and estimated amounts of removed Cenozoic cover in the northern part of the Central Tertiary Basin that were similar to those of Manum and Throndsen (1977). Within the West Spitsbergen Fold Belt, they found that the variation in coal rank with stratigraphic level differed from that in the Central Tertiary Basin and argued that this could be due to the compressional tectonics in this region.

Marshall et al. (2015) studied the maturity of coal in the Firkanten Formation and estimated its maximum burial as 2 km, 1 km of which has been removed by erosion. Their preferred paleogeothermal gradient (50°C/km) is much higher than the end-Eocene gradients determined in this study (Fig. 9), leading to significantly lower estimates of erosion than those presented here. Note that our data define an end-Eocene gradient similar to the present-day gradients measured in the wells studied (c. 30°C/km; Fig. 9c). Furthermore, a review of geothermal gradients measured in Svalbard wells show that the gradients are mostly around 30–35°C/km and that higher values are rare (Olaussen et al., 2022). This suggests that our value is reliable.

Blythe and Kleinspehn (1998) reported apatite fission-track data in samples from Svalbard and interpreted the data in terms of three episodes of post-70 Ma exhumation that are consistent with those presented here. Dörr et al. (2019) arrived at a similar conclusion based on low-temperature thermochronology data in samples from northern Svalbard. Dörr et al. (2018) also presented low-temperature thermochronology data in samples from Central Tertiary Basin boreholes. Their interpretation is at odds with our results and with those presented by Blythe and Kleinspehn (1998). We suspect that this may be due in part to the inclusion by Dörr et al. (2018) of apatite (U-Th-Sm)/He thermochronology (AHe), which is prone to uncertainty due to a range of complicating factors (Green and Duddy, 2018).

Green and Duddy (2010) presented interpretations of AFTA and VR data from wells in the Barents Sea which defined three episodes of cooling beginning in the intervals 65–55 Ma (Paleocene), 40–30 Ma (Eocene–Oligocene) and 10–5 Ma (late Miocene). The earliest of these episodes was defined only in the north-eastern part of the Barents Sea, whereas the two younger episodes were defined across the entire region. However, the new interpretations presented here suggest it is more likely that the earliest episode represents the effects of the event responsible for the Albian – mid-Paleocene hiatus on Svalbard, which we attribute to regional Maastrichtian exhumation. The presence of a major sub-Paleocene unconformity in the Hammerfest Basin in the south-western Barents Sea (Henriksen et al., 2011) suggests that the Maastrichtian exhumation episode also affected most of the Barents Sea.

4.3. Arctic Canada

Arne et al. (1998, 2002) reported apatite fission-track and VR data from various outcrop locations and exploration wells on Axel Heiberg and Ellesmere Islands in the eastern parts of the Sverdrup Basin that were most affected by the Eurekan Orogeny. They reported Paleocene cooling in the cores of anticlines or the hanging walls of thrust faults and attributed the cooling to denudation of structures during the Eurekan Orogeny. These results suggest a distinction between Maastrichtian regional exhumation and mid-Paleocene localised exhumation related to thrusting and inversion along major fault zones associated with the early stage of the Eurekan Orogeny.

Vamvaka et al. (2019) reported apatite fission-track and AHe data in samples from Ellesmere Island. They reported apatite fission-track ages between 50 and 40 Ma, while He-ages in individual grains showed a much wider range, from which they selected certain values that they used to derive thermal history constraints.

Fig. 9. Paleothermal data from the Reindalspasset (well R) and Sysselmannbreen (well S) boreholes defining burial and exhumation histories for the Central Tertiary Basin on Svalbard (locations in Fig. 4b). (a) AFTA parameters for samples plotted against sample depth and present-day temperatures for the two boreholes. The solid line in the left panel shows the increasing stratigraphic age with depth. The dashed lines show the predicted patterns of fission-track age and mean track length, respectively, for apatites containing < 0.1, 0.5, 1.0, and 1.5 wt% Cl from the Default Thermal History (DTH), which is the history expected if samples have not been hotter than their present-day temperature after deposition. The DTH was derived from the preserved sedimentary section and the present-day thermal gradient calculated from corrected borehole temperatures in each well. In all but one of the samples, measured ages are significantly younger than expected from the DTH scenario, showing that the section intersected in each well has been heated beyond the present-day temperature and subsequently cooled at some time after deposition. (b) Paleotemperature constraints from AFTA and VR data for the Maastrichtian, end-Eocene and late Miocene paleothermal episodes (Table 1). Legend for the stratigraphic columns in Fig. 4. Constraints for each episode in both wells define linear profiles, subparallel to the present-day temperature profile but offset to higher paleotemperatures compared to the present-day temperature profile. This is characteristic of heating due predominantly to deeper burial. Maximum post-depositional paleotemperatures derived from VR data are consistent with the maximum paleotemperatures defined from AFTA (Maastrichtian in borehole R and end-Eocene in borehole S). (c) Ranges of allowed paleo-gradients and removed section (hyperbolic ellipsoids) required to explain paleothermal profiles in the two boreholes within 95% confidence limits. Surface temperature: 20°C Maastrichtian and end-Eocene, 10°C late Miocene. Interpretations based on constant geothermal gradients corresponding to the present-day conditions for the well R and for the late Miocene episode in well S are also indicated (vertical lines). The present-day thermal gradient of 30°C/km in borehole S lies at the extreme of the allowed range for the end-Eocene event, and it is possible that the paleogeothermal gradient in this well, when cooling began at c. 35 Ma, may have been slightly higher than the present-day value, as indicated.

From a combination of apatite fission-track and AHe data in their basement samples, Vamvaka et al. (2019) presented a scenario involving three periods of cooling in the intervals 55–48 Ma, 44–38 Ma, and 34–26 Ma, showing close correspondence to the two stages of the Eurekan Orogeny and the subsequent post-Eurekan stage defined by Piepjohn et al. (2016). However, we note from the supplementary information presented by Vamvaka et al. (2019) that their solutions were artificially constrained to begin cooling from temperatures between 140 and 160°C between 60 and 50 Ma. This cooling episode is broadly consistent with the Paleocene cooling episode defined from our AFTA in the Wandel Sea Basin. We consider it likely that the Paleocene cooling required to explain the Canadian results shared a common origin with that detected in this study in North Greenland, although Vamvaka et al. (2019) considered the Paleocene cooling to have a non-tectonic origin.

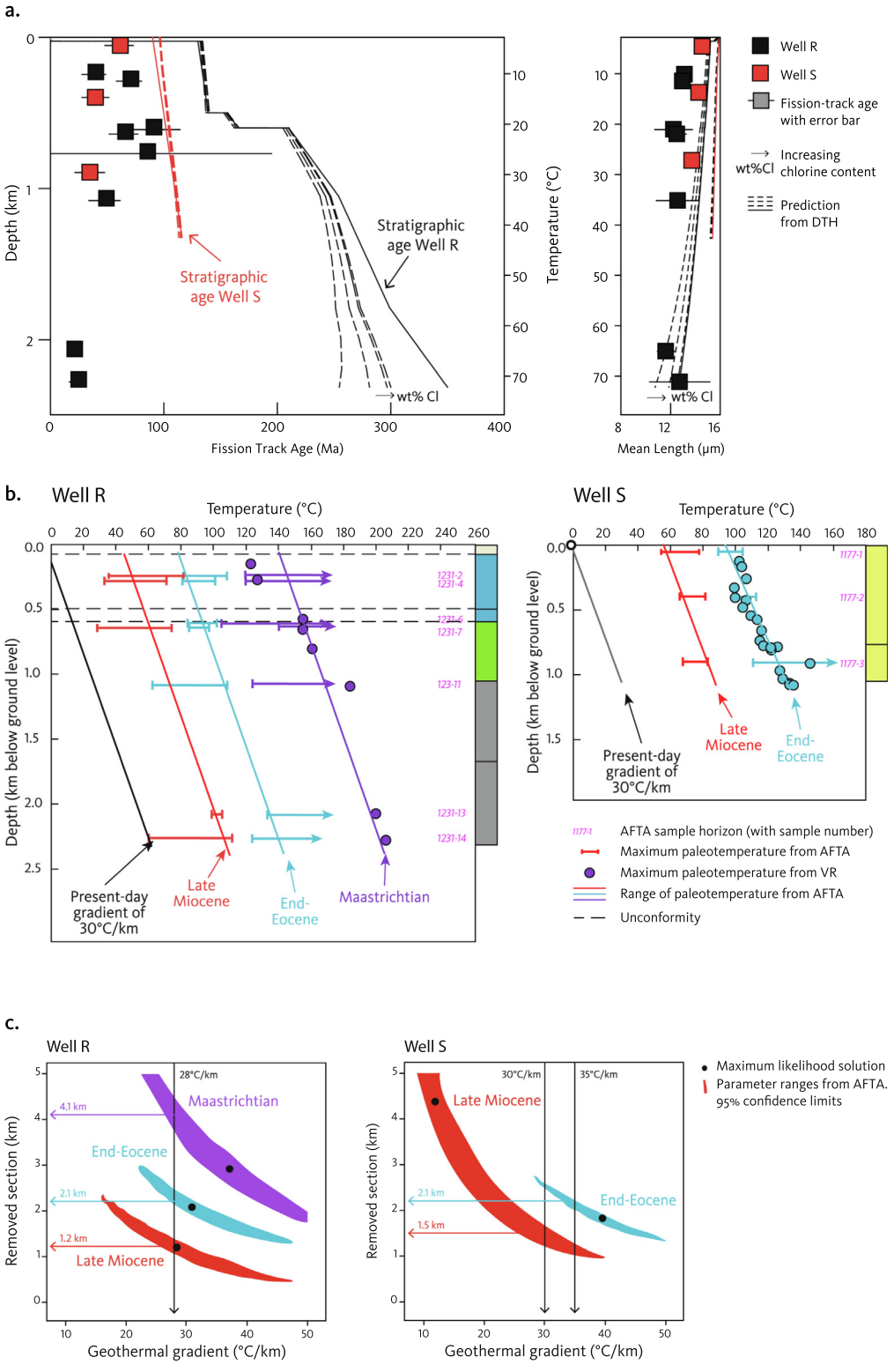

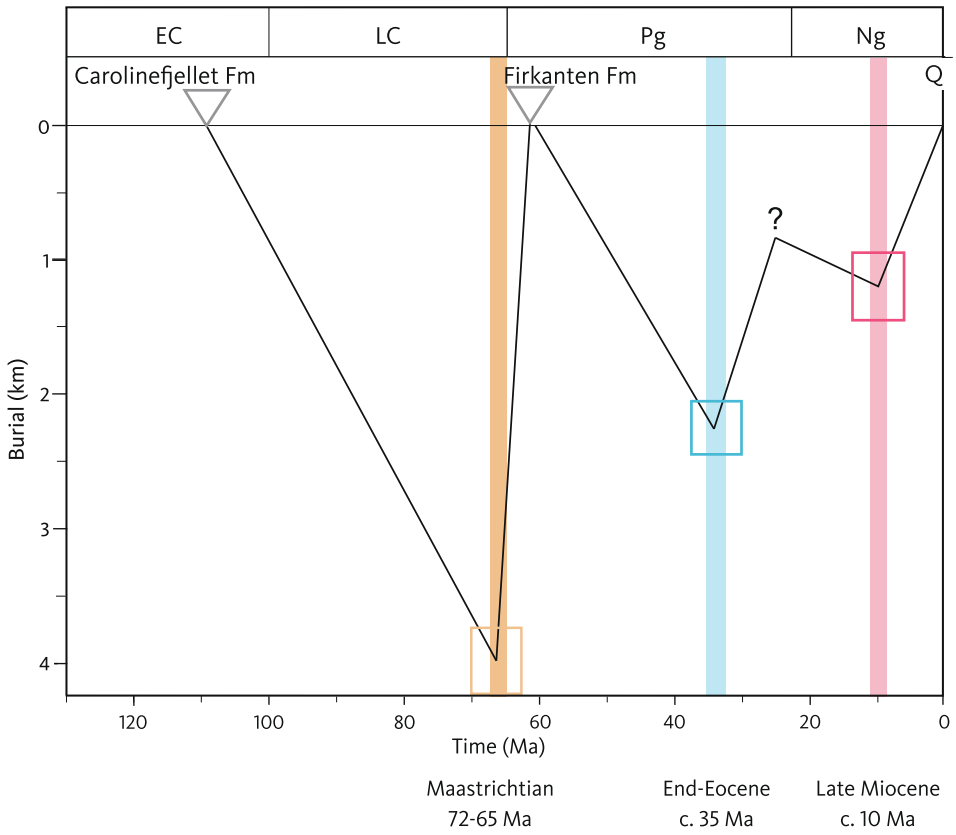

Fig. 10. Reconstructed burial and exhumation history for a sample of the Lower Cretaceous Carolinefjellet Formation adjacent to an outcrop of the mid-Paleocene Firkanten Formation in the Central Tertiary Basin, Svalbard (based on the interpretation of the paleothermal data from the Reindalspasset and Sysselmannbreen boreholes in Fig. 9). The reconstruction shows that a Cretaceous succession of about 4.3 km was deposited and then removed during Maastrichtian exhumation at the location of the Reindalspasset borehole. A mid-Paleocene – Eocene succession of c. 2.1 km was then deposited at the locations of both boreholes prior to end-Eocene exhumation. That succession was removed after end-Eocene and late Miocene exhumation. The mid-Cretaceous episode of cooling and exhumation (beginning between 118 and 95 Ma) is not shown because the focus of the paper is on the Cenozoic exhumation history. Triangles indicate assumed conditions at the surface. EC: Early Cretaceous. LC: Late Cretaceous. Pg: Paleogene. Ng: Neogene. Q: Quaternary.

We consider it unlikely that the data presented by Vamvaka et al. (2019) could independently define three cooling episodes between 55 and 26 Ma in addition to the imposed cooling between 60 and 50 Ma, particularly since their selection of He-ages to include in the modeling lacks independent control (Green and Duddy, 2018). Instead, we suggest that a more reasonable interpretation would be two major cooling episodes beginning at c. 60 and c. 35 Ma, as in North Greenland. Late Cretaceous–Paleocene cooling defined from detrital ages in Paleocene sandstones by Vamvaka et al. (2019) is consistent with the Maastrichtian cooling defined in Svalbard in this study.

In summary, we suggest that the thermochronology studies of Arne et al. (1998, 2002) and Vamvaka et al. (2019) provide evidence of a history of exhumation in the eastern part of the Sverdrup Basin which is similar to that defined here for the Wandel Sea Basin and on Svalbard, in terms of Maastrichtian, Paleocene and end-Eocene episodes of exhumation. Further evidence for this suggestion comes from the presence of significant late Maastrichtian, mid-Paleocene and end-Eocene unconformities in the Canadian High Arctic dated at 68, 62 and 34 Ma (Fig. 3; Ricketts 1994; Embry et al., 2018). Studies of thermochronology and of stratigraphy in the eastern Sverdrup Basin thus provide evidence for (1) regional Maastrichtian exhumation that led to the formation of a pronounced base-Paleocene unconformity before subsidence in wide areas across the Sverdrup Basin, (2) mid-Paleocene exhumation during inversion of fault zones in Stage 1 of the Eurekan Orogeny and (3) regional exhumation beginning at the end of the Eocene. Green and Duddy (2010) reported evidence from AFTA for widespread Paleocene, end-Eocene and Miocene exhumation across the North American Arctic.

4.4. Arctic Ocean

AFTA data in dredge samples from the Lomonosov Ridge (c. 89°N) defined cooling which began in the intervals 95–62 Ma and 26–4 Ma (Knudsen et al., 2017). These intervals are consistent with the Maastrichtian cooling episode identified on Svalbard and in the Sverdrup Basin and with the regional, late Miocene cooling episode. The 400-m ACEX drillcore obtained from an adjacent location (c. 88°N) on the Lomonosov Ridge terminated in upper Paleocene sediments and penetrated a 26 Myr mid-Cenozoic hiatus, separating middle Eocene from lower Miocene sediments and a 2 Myr unconformity in the late Miocene (Backman et al., 2008). It is possible that the mid-Cenozoic hiatus is the result of the regional, end-Eocene episode of exhumation described here, although that episode of cooling and exhumation was not resolved in the AFTA data from the dredge samples. However, the late Miocene hiatus in the drillcore corresponds closely to the regional late Miocene episode of exhumation which is confirmed by the AFTA data from the dredge samples. This correlation is further confirmed by an up to 8 Ma ferromanganese crust on the dredge samples that Knudsen et al. (2017) considered to represent outcrop conditions, corresponding to exhumation of the samples during the late Miocene episode of uplift and erosion.

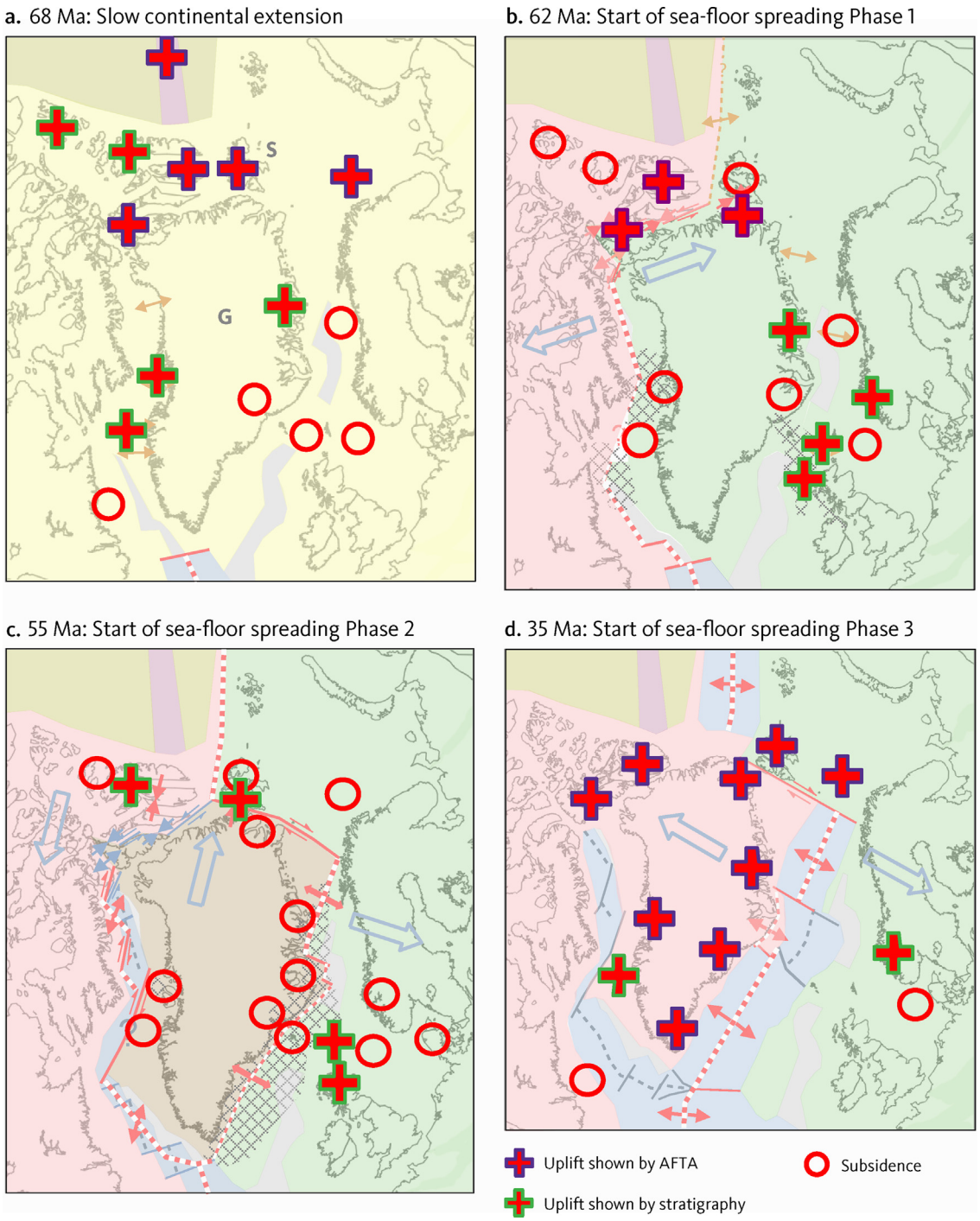

Fig. 11. Areas of uplift and subsidence around the North-East Atlantic from the Maastrichtian to the end of the Eocene superimposed on the plate reconstructions shown in Fig. 2. The full legend is shown in Fig. 2. (a) Starting at 68 Ma, late Maastrichtian: Uplift and erosion resulted in a pronounced unconformity in the High Arctic and across wide areas west of Greenland. Subsidence between Greenland and Eurasia. Sources: Balkwill (1987); Bjerager et al. (2020); Embry and Beauchamp (2019); Evans (2003); Henriksen et al. (2011); Japsen et al. (2005, 2014); Larsen and Whitham, 2005; Stoker et al. (2017) and this paper. (b) Starting at 62 Ma, mid-Paleocene: Subsidence dominated onshore and offshore East and West Greenland following initial uplift that decreased away from the main areas of volcanism. Subsidence in the western Canadian Archipelago and Svalbard formed foreland basins. Uplift in western Scotland and in southern west Norway probably occurred in response to the movement of plume material under these areas. Inversion of fault zones on Ellesmere Island and in North Greenland. Sources: Dalhoff et al. (2003); Embry and Beauchamp (2019); Green et al. (2013); Holford et al. (2010); Jones et al. (2017); Nielsen et al. (1981); Nøhr-Hansen et al. (2011); Stoker et al. (2017); Sømme et al. (2019); White and Lovell (1997) and this paper. (c) Starting at 55 Ma, earliest Eocene: Much of Greenland subsided. Subsidence in the North Sea and across southern Scandinavia, waves of uplift and subsidence in the Faroe – Shetland Basin. Sources: Dalhoff et al. (2003); Dallmann (2015); Green et al. (2013); Harrison (2008); Heilmann-Clausen et al. (1985); Henriksen et al. (2011); Japsen et al. (2014, 2018, 2021b); Piepjohn et al. (2016); White and Lovell (1997). (d) Starting at 35 Ma, late Eocene: Uplift and erosion of all margins along Greenland and in the High Arctic. Minor uplift of southern Norway. Sources: Balkwill (1987); Green and Duddy (2010); Green et al. (2014); Japsen et al. (2006, 2007 and references therein, 2010, 2014, 2021b) and this paper. (For interpretation of the references to colour in this figure legend, the reader is referred to the web version of this article.)

5. Latest Cretaceous – Neogene tectonics

5.1. Maastrichtian exhumation – Possible doming above the rising Iceland plume (Fig. 11a)

Evidence from thermochronology and stratigraphy shows that Maastrichtian uplift and erosion affected a huge area across Greenland, the North American Arctic to Svalbard, the Barents Shelf and the Lomonosov Ridge (Figs. 3, 11a):

- Ricketts (1994) reported that latest Cretaceous uplift was widespread in the North American Arctic, and this observation is supported by evidence for cooling and exhumation from the eastern Sverdrup Basin (Arne et al., 2002; Vamvaka et al., 2019; Section 4.3). Uplift and erosion led to the formation of a Maastrichtian unconformity that is recognized across the Canadian High Arctic (dated at 68 Ma; Embry et al., 2018). The Maastrichtian unconformity in the Sverdrup Basin is more pronounced towards Greenland (Ricketts, 1994).
- In the Wandel Sea Basin, a significant hiatus separates the youngest, well-dated Upper Cretaceous sediments of Santonian age from the exposed upper Paleocene deposits in Kronprins Christian Land (Lyck and Stemmerik, 2000; Hovikoski et al., 2018), suggesting that Maastrichtian exhumation may also have affected this region. Further west, the presence of the Kap Washington volcanics and interbedded shales of Maastrichtian age (Tegner et al., 2011) suggests that Maastrichtian exhumation may not have been pronounced in north-west Peary Land. The AFTA data do not, however, resolve definite evidence of Maastrichtian cooling, possibly because any such effects were overprinted by the high temperatures during subsequent paleo-thermal episodes.
- A Maastrichtian unconformity is an important marker on– and off-shore West and North-East Greenland (Japsen et al., 2005; Bjerager et al., 2020; Fyhn et al., 2021). Off North-East Greenland, late Maastrichtian sediments, derived from the uplifted Greenland, prograded eastwards above this unconformity (Fyhn et al., 2021). Some of these sediments may have reached as far as the Vøring Basin off mid-Norway (Fjellanger et al, 2005). The uplift was accompanied by faulting in present-day central West Greenland and an increased input of sediment from the uplifted hinterland eroded sub-sea canyons in the crests of the fault blocks (Dam and Sønderholm, 1998; Dam and Nøhr-Hansen, 2001).
- Exhumation on Svalbard (onset 72–65 Ma; Table 1) led to the formation of the Albian – mid-Paleocene hiatus in the Central Tertiary Basin. We infer that the Maastrichtian – mid-Paleocene hiatus across the south-western Barents Shelf also represents this episode (Henriksen et al., 2011; Jones et al., 2017). The formation of the base-Paleocene unconformity of the Central Tertiary Basin involved the removal of about 4 km of Cretaceous sediments at the location of the Reindalspasset borehole (Figs. 9, 10).
- Late Cretaceous – early Paleocene cooling (onset 95–62 Ma) is observed in dredge samples from the Lomonosov Ridge (Knudsen et al., 2017). We interpret this result as evidence of Maastrichtian exhumation reaching as far north as the North Pole.

The results from the low-temperature thermochronology presented here and the age of the late Maastrichtian unconformity in the Canadian High Arctic (Embry et al., 2018) show that regional Maastrichtian uplift and erosion in the High Arctic began at c. 68 Ma.

The Maastrichtian episode of regional exhumation thus predates the mid-Paleocene onset of sea-floor spreading west of Greenland and the onset of eruption of the picritic lavas in West Greenland at 62 Ma that is commonly taken as the sign of the impact of the Iceland plume head on the lithosphere (see Section 2.2). The area affected by the uplift was at least 2000 km in diameter (Fig. 11a). We therefore hypothesise that the Maastrichtian uplift reflects doming above the rising Iceland Plume upon its arrival in the upper mantle, prior to its impact at the base of the lithosphere. In support of this hypothesis, we cite Campbell (2007) who showed evidence that pre-impact doming can become evident 3 to 10 Myr before plume impact, and that the diameter of the dome can be of the order of 1000 to 2000 km. If this hypothesis is correct, then the time lag is 6 Myr between the onset of Maastrichtian pre-impact doming (68 Ma; Embry et al., 2018) and the mid-Paleocene impact itself at 62 Ma. Our hypothesis is consistent with the placing of the rising plume head under central northern Greenland (O'Neill et al., 2005; Celli et al., 2021). It is marginally consistent with placing of the plume head under central West Greenland (Lawver and Müller, 1994) and inconsistent with the placing under central East Greenland (Doubrovine et al., 2012; Barnett-Moore et al., 2017).

5.2. Mid-Paleocene exhumation of inverted fault zones – Eurekan Stage 1 driven by the movement of Greenland relative to North America (Fig. 11b)

Stage 1 of the Eurekan Orogeny in late Paleocene times affected wide areas in the High Arctic involving inversion of fault zones, thrusting and formation of foreland basins (represented by the onset of deposition of the sandstones of the upper Expedition Formation in the Sverdrup Basin, the Thyra Ø Formation in the Wandel Sea Basin and the Firkanten Formation in the Central Tertiary Basin; Fig. 3).

The north-eastward movement of Greenland relative to North America in the late Paleocene was taken up on a series of strike-slip faults on Ellesmere Island (Harrison, 2004; Oakey and Chalmers, 2012). Thrusting on the step-overs between these faults caused folding, thrusting and uplift in parts of the Sverdrup Basin (Harrison, 2004). These movements correspond to Stage 1 of the Eurekan Orogeny (Fig. 11b). Thermochronological data from the eastern Sverdrup Basin provide evidence for localised exhumation related to Paleocene thrusting and inversion (Arne et al., 2002; Vamvaka et al., 2019; Section 4.3).

The style of deformation in the fault zones of the Wandel Sea Basin has been interpreted as the result of Paleocene–Eocene N-S directed compression (Svennevig et al., 2016). The Eurekan deformation, however, took place in two stages, as discussed in Section 2 (Figs. 2b,c). During the Paleocene Stage 1, the SSW–NNE movement of Greenland relative to Svalbard gave rise to compression (beginning between 60 and 57 Ma; Table 1) that caused inversion and exhumation along the fault zones and contributed to the present-day outline of the Wandel Sea Basin with scattered sedimentary outliers.

The West Spitsbergen Fold Belt formed as initial SSW-NNE compression followed by minor transpressional modifications (Manby and Lyberis, 1996; Bergh et al., 1997). This is consistent with the SSW-NNE movement of Greenland in the Paleocene followed by the Eocene transpression along the De Geer Line (Figs. 2c,d). We therefore conclude that the SSW-NNE Paleocene compression caused the formation of the West Spitsbergen Fold Belt and the onset of subsidence of the Central Tertiary Basin as a foreland basin. The AFTA data available from Svalbard provide no evidence of Paleocene cooling, although this could simply be due to the lack of samples in areas affected by tectonism.

The results from low-temperature thermochronology presented here and the age of the mid-Paleocene unconformity in the Canadian High Arctic (Embry et al., 2018) lead us to suggest that the

Paleocene inversion of the fault zones in the eastern Sverdrup Basin, in the Wandel Sea Basin and in the West Spitsbergen Fold Belt all began at c. 62 Ma.

A case can be made, as suggested by Harrison et al. (1999; see also Stotz et al., 2018) that outflow from the mantle plume was a significant, if not the primary, driving force for the increase in velocity of separation between the North American and Greenland-Eurasia plates. This force eventually led to sea-floor spreading in the Labrador Sea and Baffin Bay and thus contributed to the onset of the Eurekan Orogeny. The mid-Paleocene impact of the Iceland Plume on the base of the lithosphere under Greenland happened during slow, intra-continental extension around Greenland (Chian and Louden, 1994; Fyhn et al., 2021), and the situation thus corresponds to the 'semi-active' mode of continental rifting and break-up defined by Koptev et al. (2021) based on numerical experiments. The 'semi-active' mode is characterized by *syn*-breakup volcanism carrying the geochemical signatures of the deep mantle, which agrees with the mid-Paleocene onset of high-temperature picritic volcanism on– and offshore West Greenland (Pedersen et al., 2017; Riisager er al., 2003; Larsen and Williamson, 2020).

Many models of plume impact, predict an elevated land surface after the impact (e.g. François et al., 2018; Koptev et al., 2021). Observations show, however that after a very short-lived uplift, there was rapid subsidence in both East and West Greenland, starting immediately after the onset of volcanic eruptions at the time of plume impact (Pedersen et al., 2002; Larsen and Tegner, 2006; Dam et al., 2009; Green et al 2013, chapter 5). In central East Greenland (68–70^{0}N), for example, subsidence during the eruption of the basalts at the time of break-up (c. 56 Ma), kept pace with the outpouring lavas, so that the land surface at the end of the eruptions remained at or near sea level (Brooks and Nielsen, 1982; Bonow et al., 2014). The tectonic regime at that time was extensional, and this resulted in subsidence of the base of the basalts, so that there was balance between subsidence and accumulation because of the easy access from magma chambers in the crust to the eruption sites. In central West Greenland, uplift immediately preceding the first eruptions was followed shortly afterwards by several hundreds of meters of subsidence forming a basin into which lavas prograded forming a Gilbert delta (Pedersen et al., 1993; Green et al., 2013).

5.3. Eocene tectonics: Eurekan Stage 2 (Fig. 11c)

Sea-floor spreading started between Greenland and Eurasia in the earliest Eocene and sea-floor spreading in the Labrador Sea and Baffin Bay continued after a change in spreading direction (Figs. 2b,c). These changes caused Greenland to move northwards relative to both Ellesmere Island and Svalbard. The result of these movements on Ellesmere Island was large-scale, south-directed thrusting and deposition of *syn*-tectonic conglomerates (Buchanan Lake Fm) in front of the advancing thrust sheets in the mid-Eocene (Ricketts, 1994; Embry and Beauchamp, 2019; Fig. 1). The crustal shortening destroyed the contiguous Sverdrup Basin and, in its place, produced several small intermontane basins which, in several cases, were associated with major thrust systems (Ricketts, 1994). Major arches, hundreds of kilometers in length, formed further west that have been modelled as large, continental, crustal-scale folds that formed during the main phase of Eurekan crustal shortening (Stephenson et al., 1990). Oakey and Chalmers (2012) showed that the folds solved a space problem caused by the northward movement of Greenland relative to North America during the Eocene. Ricketts and Stephenson's (1994) showed that arch uplift was transitional between the final stages of subsidence in the Sverdrup Basin and maximum crustal failure of the overthrust area farther east.

Sea-floor spreading also started in the Arctic Ocean in the latest Paleocene (C25) (Brozena et al, 2003) or more likely in the earliest Eocene (C24) (Jokat et al., 2016) at the same time as sea-floor spreading started between Greenland and Eurasia. This caused the trajectory of Svalbard relative to Greenland to change from compressional to dextral transpression along the De Geer Line. The West Spitsbergen Fold Belt on Svalbard was modified during the early Eocene by minor dextral transpression due to movement along the De Geer Line (Manby and Lyberis, 1996; Bergh et al., 1997; Steel et al., 1985; Dallmann, 2015 and references therein; See Section 2).

Neither our data nor any published results from thermochronology of which we are aware reveal any paleo-thermal effects related to published times of major tectonic activity during the Eocene Stage 2 of the Eurekan Orogeny (Tegner et al., 2011; Embry et al., 2018). This may be because the amounts of denudation were relatively small, and/or localised to discrete structures which we have not sampled in this study. Widespread areas across the High Arctic subsided during the Eocene, leading to accumulation of thick sedimentary successions prior to the onset of exhumation at the end of the Eocene, as we discuss in the subsequent Section.

5.4. Exhumation episodes postdating the Eurekan Orogeny (Fig. 11d)

5.4.1. Exhumation beginning at the end of the Eocene

Cooling reflecting exhumation that began at the end of the Eocene (c. 35 Ma) affected the Wandel Sea Basin and Svalbard and correlates with the Oligocene hiatus in these areas and with a base-Oligocene, angular unconformity of tectonic origin in the Canadian High Arctic dated at 34 Ma (Figs. 3, 11d; Embry et al., 2018). This episode of regional denudation began around the time that sea-floor spreading west of Greenland had ended (C13, 33 Ma) and thus post-dates the Eurekan Orogeny. The difference between these estimated times is small, however, and we refer to the onset of cooling at this time as 35 Ma (end-Eocene).

A sedimentary succession about 2 km thick was removed from wide areas across the Wandel Sea Basin and from the region around the Central Tertiary Basin on Svalbard. Both regions had subsided during the Eocene and, in many places, the removed section consisted of Eocene sediments. The Paleocene–Eocene deformation of the Sverdrup Basin climaxed in the late Eocene and the entire basin was uplifted, 'bringing to a close a 300-million-year history of deposition' (Embry and Beauchamp, 2019). Exhumation beginning at the end of the Eocene also affected the Barents Sea, the north slope of Alaska (Green and Duddy, 2010) and in all areas of Greenland where exhumation has been studied to date (Fig. 11d; references in the caption to Fig. 11d).

There is a clear offset in the end-Eocene paleotemperatures across the Harder Fjord Fault Zone in northern Peary Land, North Greenland (Figs. 1, 8b). This offset indicates reverse faulting where the northern side of the fault zone was uplifted about 1 km more than the area south of the fault (Japsen et al., 2021), confirming the observation that N-S compression resulted in reverse faulting in northern Peary Land in post-late Santonian times (Piepjohn and von Gosen, 2001). However, Piepjohn and von Gosen (2001) interpreted this compression to be part of the Eurekan Orogeny, whereas our results show that the inversion of the Harder Fjord Fault Zone took place in two episodes; one that began during the Paleocene and another that began at the end of the Eocene. Unlike the first episode that represents the onset of the Eurekan Orogeny, the second episode represents post-Eurekan tectonics.

Uplift and erosion in the High Arctic that began at the end of the Eocene, close to the time when (1) sea-floor spreading west of Greenland had terminated at C13 time, (2) a minimum of the rate of sea-floor spreading and a significant change in spreading direc-

tions in the North-East Atlantic took place also at C13 time (Gaina et al., 2017) and (3) exhumation began in East and West Greenland, far from the Eurekan Orogen.

These observations indicate that a deep-rooted, tectonic process began in the North-East Atlantic at the end of the Eocene, subsequent to the Eurekan Orogeny. Gaina et al. (2017) noted that the continental margins of North America and Eurasia underwent massive changes in the late Eocene–Oligocene and suggested that the European Plate probably changed direction of absolute motion due to successive adjustments along its southern boundary. Such changes may have resulted in a reorientation in intra-plate stresses causing re-adjustments of the rate of seafloor spreading observed at the Eocene–Oligocene transition.

Dewey et al. (1989) also identified a major change in tectonic phases at C13 time in the western Mediterranean from a model that used a study of Atlantic fracture zones to integrate the motion of Africa relative to Europe. These changes at the southern margin of Europe may have generated forces that were transmitted across the spreading center north-west of Europe, through the asthenosphere (Höink et al., 2012; Colli et al., 2018). Could transmission of this stress have contributed to both major plate-tectonic changes in the North-East Atlantic and to uplifts in Greenland and surrounding regions at the Eocene–Oligocene transition?

5.4.2. Exhumation beginning in the late Miocene

An additional episode of post-Eurekan uplift and erosion started in the late Miocene (c. 10 Ma; Table 1) and affected wide areas across the High Arctic, including the Lomonosov Ridge and the conjugate margins of the Fram Strait (Green and Duddy, 2010; Knudsen et al., 2017; Dörr et al., 2019; Japsen et al., 2021a, b). Off North-East Greenland, massive shelf progradation occurred above a distinct angular, intra-Miocene unconformity (IMU) that Døssing et al. (2016) dated to be middle to late Miocene (15–10 Ma). The IMU marks the termination of synrift deposition in the deep-sea basins and the onset of contourite deposition south of the Fram Strait. Japsen et al. (2021b) therefore suggested that the uplift onshore and the uplift that formed the IMU represent the same late Miocene episode that began at 10 Ma. The prograding sediments deposited above the IMU show that the onshore area remained uplifted and provided the sediment source while the offshore area subsided.

The late Miocene uplift initiated the formation of the present-day, elevated landscapes in Greenland and Svalbard (Dörr et al., 2019; Japsen et al., 2021b). The Barents Sea was also affected by late Miocene exhumation (Green and Duddy, 2010), but here the end-result was a submerged shelf. In contrast to the High Arctic, Neogene uplift and erosion in Scandinavia began in the early Miocene (Fig. 7b) at approximately the same time as sea-floor spreading started between Jan Mayen and Greenland (Gaina et al., 2009). Japsen et al. (2021b) speculated that late Neogene changes in the absolute motion of the North American Plate may explain this asymmetric behavior across the North-East Atlantic. Sea-floor spreading rates between Eurasia – North America and Nubia – North America varied modestly from 20 to *c.* 8 Ma but slowed down by *c.* 20% between 8 and 5 Ma, and the rates have remained remarkably steady since then (Merkouriev & DeMets 2008; DeMets et al. 2015; Iaffaldano & DeMets 2016). These changes in relative motions were related to a change in the absolute motion of North America and Antarctica, and they might be linked to the late Neogene dynamics of the Pacific Plate (Iaffaldano & DeMets 2016).

6. Summary

We have integrated new and published low-temperature thermochronology data with stratigraphic information from disparate parts of the High Arctic and have – for the first time - identified four episodes of synchronous cooling and exhumation during the latest Cretaceous – Neogene. Three of the episodes are regional and started both before and after the Eurekan Orogeny that was induced by the late Paleocene – Eocene movement of Greenland relative to the North American and Eurasian plates:

1. Regional Maastrichtian uplift and erosion that began at c. 68 Ma affected the Canadian High Arctic, Svalbard, the Barents Sea, the Lomonosov Ridge and parts of Greenland, both onshore and offshore. We hypothesise that this episode of uplift reflects doming above the rising head of the Iceland Plume upon its arrival in the upper mantle and prior to its impact at the base of the lithosphere under Greenland at c. 62 Ma.
2. Localised Paleocene exhumation that began at c. 62 Ma resulted from inversion of fault zones in the Wandel Sea Basin and in the eastern Sverdrup Basin. These uplifts occurred while Greenland moved together with Eurasia relative to North America causing local compression on Ellesmere Island and Svalbard leading to the inversion of fault zones. We show that the folding that caused the West Spitsbergen Fold Belt is consistent with this Paleocene movement and was not caused by transpression during the Eocene as many authors have assumed. The compression also formed foreland basins such as the Central Tertiary Basin. Paleo-thermal effects of this episode are as yet undetected in Svalbard, possibly due to the available data coverage. This episode started when the Iceland Plume impacted the lithosphere under Greenland, possibly contributing to the onset of sea-floor spreading west of Greenland and that provided the driving force for the Eurekan Orogeny.
3. Regional exhumation that began at the end of the Eocene (c. 35 Ma) affected wide regions extending from south Greenland across the High Arctic, including areas far beyond those involved in the Eurekan deformations. The onset of this episode took place close to the cessation of sea-floor spreading west of Greenland, and it thus represents post-Eurekan tectonics. The onset of this episode of exhumation also coincided with a minimum of the rate of sea-floor spreading and a significant change in the spreading directions in the North-East Atlantic. Is it possible that these changes were caused by the major shift in the motion of Africa relative to Europe that also happened at this time?
4. Regional, late Miocene uplift and erosion that began at c. 10 Ma affected wide areas across the High Arctic, including the conjugate margins of the Fram Strait and the Lomonosov Ridge, close to the North Pole. This episode initiated the formation of the present-day elevated landscapes of Greenland and Svalbard, but in the Barents Sea the end-result was a submerged shelf. The forces driving this episode may be linked to changes in the absolute motion of North American Plate.

We have not detected exhumation within the area of the Eurekan Orogeny during the Eocene, when Greenland moved northwards separately from both North America and Eurasia. This may reflect the available data coverage but may also be because widespread areas in the High Arctic subsided during the Eocene leading to accumulation of thick siliciclastic successions.

The results presented here illustrate the complex interplay of tectonic forces responsible for subsidence and uplift that eventually leads to deposition and to removal of rocks and thus to obliteration of part of the stratigraphic record. Our study emphasizes the importance of investigating evidence of sedimentary sequences that were once deposited and subsequently removed (missing section) from the preserved geological record. By doing so, it is possible to gain a better understanding of the geological development and of the tectonic forces driving horizontal and vertical move-

ments of the earth's crust. It is now important to investigate the interplay of the tectonic forces by geodynamic modelling, constrained by observations of the vertical movements of the crust, such as those presented here.

CRediT authorship contribution statement

Peter Japsen: Conceptualization, Data curation, Project administration, Investigation, Writing – original draft, Writing – review & editing. **Paul F. Green:** Formal analysis, Methodology, Investigation, Writing – original draft, Writing – review & editing. **James A. Chalmers:** Formal analysis, Investigation, Writing – review & editing.

Declaration of Competing Interest

The authors declare that they have no known competing financial interests or personal relationships that could have appeared to influence the work reported in this paper.

Acknowledgements

We are grateful for the economic support for this study provided by Equinor ASA and GEUS. We thank Torbjørn Dahlgren for his wholehearted support of the study, as well as five anonymous reviewers and Editor Taras Gerya for their constructive comments.

Appendix A. Supplementary data

Supplementary data to this article can be found online at https://doi.org/10.1016/j.gr.2023.01.011.

References

Abay, T.B., Karlsen, D.A., Pedersen, J.H., Olaussen, S., Backer-Owe, K., 2017. Thermal maturity, hydrocarbon potential and kerogen type of some Triassic – Lower Cretaceous sediments from the SW Barents Sea and Svalbard. Pet. Geosci. 24, 349–373. https://doi.org/10.1144/petgeo2017-035.

Arne, D., Zentilli, M., Grist, A., Collins, M., 1998. Constraints on the timing of thrusting during the Eurekan orogeny, Canadian Arctic Archipelago: an integrated approach to thermal history analysis. Can. J. Earth Sci. 35, 30–38. https://doi.org/10.1139/cjes-35-1-30.

Arne, D., Grist, A., Zentilli, M., Collins, M., Embry, A., Gentzis, T., 2002. Cooling of the Sverdrup Basin during Tertiary basin inversion: implications for hydrocarbon exploration. Basin Res. 14, 183–205. https://doi.org/10.1046/j.1365-2117.200.00163.x.

Atkinson, D.J., 1963. Tertiary Rocks of Spitsbergen. AAPG Bull. 47, 302–323. https://doi.org/10.1306/bc743987-16be-11d7-8645000102c1865d.

Backman, J., Jakobsson, M., Frank, M., Sangiorgi, F., Brinkhuis, H., Stickley, C., O'Regan, M., Lovlie, R., Palike, H., Spofforth, D., Gattacecca, J., Moran, K., King, J., Heil, C., 2008. Age model and core-seismic integration for the Cenozoic Arctic Coring Expedition sediments from the Lomonosov Ridge. Paleoceanography 23. https://doi.org/10.1029/2007PA001476.

Balkwill, H.R., 1987. Labrador Basin: structural and stratigraphic style. In: Beaumont, C., Tankard, A.J. (Eds), Sedimentary Basins and Basin-forming Mechanisms. Can. Soc. Pet. Geol., Mem., 12, 1743.

Barnett-Moore, N., Hassan, R., Flament, F., Müller, D., 2017. The deep Earth origin of the Iceland plume and its effects on regional surface uplift and subsidence. Solid Earth 8, 235–254. https://doi.org/10.5194/se-8-235-2017.

Bergh, S.G., Braathen, A., Andresen, A., 1997. Interaction of basement-involved and thin-skinned tectonism in the Tertiary fold-thrust belt of central Spitsbergen. Svalbard. AAPG Bull. 81, 637–661. https://doi.org/10.1306/522B43F7-1727-11D7-8645000102C1865D.

Bjerager, M., Alsen, P., Hovikoski, J., Lindström, S., Stemmerik, L., Therkelsen, J., 2019. Triassic lithostratigraphy of the Wandel Sea Basin, North Greenland. Bull. Geol. Soc. Denm. 67, 83–105.

Bjerager, M., Alsen, P., Bojesen-Koefoed, J., Fyhn, M.B., Hovikoski, J., Ineson, J., Nøhr-Hansen, H., Nielsen, L.H., Piasecki, S., Vosgerau, H., 2020. Cretaceous lithostratigraphy of North-East Greenland. Bull. Geol. Soc. Denm. 68, 37–93. https://doi.org/10.37570/bgsd-2020-68-04.

Blythe, A.E., Kleinspehn, K.L., 1998. Tectonically versus climatically driven Cenozoic exhumation of the Eurasian plate margin, Svalbard: Fission track analyses. Tectonics 17, 621–639. https://doi.org/10.1029/98tc01890.

Bonow, J.M., Japsen, P., Nielsen, T.F.D., 2014. High-level landscapes along the margin of East Greenland – a record of tectonic uplift and incision after breakup in the NE Atlantic. Glob. Planet. Change 116, 10–29. https://doi.org/10.1016/j.gloplacha.2014.01.010.

Brooks, C.K., Nielsen, T.F.D., 1982. The E Greenland continental margin: a transition between oceanic and continental magmatism. J. Geol. Soc. London 139, 265–275. https://doi.org/10.1144/gsjgs.139.3.02.

Brozena, J., Childers, V., Lawver, L., Gahagan, L., Forsberg, R., Faleide, J., Eldholm, O., 2003. New aerogeophysical study of the Eurasia Basin and Lomonosov Ridge: Implications for basin development. Geology 31, 825–828. https://doi.org/10.1130/G19528.1.

Campbell, I.H., 2007. Testing the plume theory. Chem. Geol. 241, 153–1117. https://doi.org/10.1016/j.chemgeo.2007.01.024.

Celli, N.L., Lebedeva, S., Schaeffer, A.J., Gaina, C., 2021. The tilted Iceland Plume and its effect on the North Atlantic evolution and magmatism. Earth Planet. Sci. Lett. 569, 13 pp. https://doi.org/10.1016/j.epsl.2021.117048.

Chalmers, J.A., Laursen, K.H., 1995. Labrador Sea: the extent of continental crust and the timing of the start of seafloor spreading. Mar. Petrol. Geol. 12, 205–217. https://doi.org/10.1016/0264-8172(95)92840-S.

Chalmers, J.A., Larsen, L.M., Pedersen, A.K.J., 1995. Widespread Paleocene volcanism around the northern North Atlantic and Labrador Sea: evidence for a large, hot, early plume head. J. Geol. Soc Lond. 152, 965–969. https://doi.org/10.1144/GSL.JGS.1995.152.01.14.

Chian, D., Louden, K.E., 1994. The continent-ocean crustal transition across the southwest Greenland margin. J. Geophys. Res. 99, 9117–9135. https://doi.org/10.1029/93JB03404.

Colli, L., Ghelichkhan, S., Bunge, H.-P., Oeser, J., 2018. Retrodictions of Mid Paleogene mantle flow and dynamic topography in the Atlantic region from compressible high resolution adjoint mantle convection models: Sensitivity to deep mantle viscosity and tomographic input model. Gondwana Res. 53, 252–272. https://doi.org/10.1016/j.gr.2017.04.027.

Croxton, C.A., Dawes, P.R., Soper, N.J., Thomsen, E., 1980. An occurrence of Tertiary shales from the Harder Fjord Fault, North Greenland fold belt, Peary Land. Rapport Grønlands Geologiske Undersøgelse 101, 61–64.

Dalhoff, F., Chalmers, J.A., Gregersen, U., Nøhr-Hansen, H., Rasmussen, J.A., Sheldon, E., 2003. Mapping and facies analysis of Paleocene – Mid-Eocene seismic sequences, offshore southern West Greenland. Mar. Petrol. Geol. 20, 945–986. https://doi.org/10.1016/j.marpetgeo.2003.09.004.

Dallmann, W. K. (Ed.), 2015. Geoscience Atlas of Svalbard: Norsk polarinstitutt, Report Series 148, Norwegian Polar Institute, Tromsø, 292 pp.

Dallmann, W.K., Otha, Y., Elvevold, S., Blomeier, D., 2002. Bedrock Map of Svalbard and Jan Mayen: Temakart. Norsk Polarsinstitutt, scale 1 (750), 000.

Dam, G., Sønderholm, M., 1998. Sedimentological evolution of a fault-controlled, Early Paleocene incised valley system, Nuussuaq Basin, West Greenland. In: Shanley, K.W., McKabe, P.J. (Eds), Relative role of eustacy, climate and tectonism in continental rocks. Soc. Econ. Pal. Min. Spec. Pub. 59, 109–121.

Dam, G., Nøhr-Hansen, H., 2001. Mantle plumes and sequence stratigraphy; late Maastrichtian–early Paleocene of West Greenland. Bull. Geol. Soc. Denm. 48, 189–207.

Dam, G., Larsen, M., Sørensen, J.C., 1998. Sedimentary response to mantle plumes: implications from Paleocene onshore successions, West and East Greenland. Geology 26, 207–210. https://doi.org/10.1130/0091-7613(1998)026<0207:SRTMPI>2.3.CO;2.

Dam, G., Pedersen, G.K., Sønderholm, M., Midtgaard, H.H., Larsen, L.M., Nøhr-Hansen, H., Pedersen, A.K., 2009. Lithostratigraphy of the Cretaceous–Paleocene Nuussuaq Group, Nuussuaq Basin, West Greenland. Geol. Surv. Denm. Greenl. Bull. 19, 171 pp. 10.34194/geusb.v19.4886

Dawes, P.R., Soper, N., 1973. Pre-Quaternary History of North Greenland: Regional Arctic Geology of the Nordic Countries. Arctic Geology. AAPG Mem. 19, 117–134.

DeMets, C., Iaffaldano, G., Merkouriev, S., 2015. High-resolution Neogene and Quaternary estimates of Nubia-Eurasia-North America Plate motion. Geoph. J. Int. 203, 416–427. https://doi.org/10.1093/gji/ggv277.

Dewey, J.F., Helman, M.L., Knott, S.D., Turco, E., Hutton, D.H.W. 1989. Kinematics of the western Mediterranean. In: Coward, M.P., Dietrich, D., Park, R.G. (Eds), Alpine Tectonics. Geol. Soc. Lond., Spec. Publ. 45, 265–283.

Dörr, N., Lisker, F., Clift, P.D., Carter, A., Gee, D.G., Tebenkov, A.M., Spiegel, C., 2012. Late Mesozoic-Cenozoic exhumation history of northern Svalbard and its regional significance: Constraints from apatite fission track analysis. Tectonophysics 514–517, 81–92. https://doi.org/10.1016/j.tecto.2011.10.007.

Dörr, N., Lisker, F., Jochmann, M., Rainer, T., Schlegel, A., Schubert, K., Spiegel, C., 2018. Subsidence, rapid inversion and slow erosion of the Central Tertiary Basin of Svalbard: Evidence from the thermal evolution and basin modelling. In: Piepjohn, K., Strauss, J.V., Reinhardt, L., McClelland, W.C. (Eds), Circum-Arctic Structural Events: Tectonic evolution of the Arctic margins and Trans-Arctic links with adjacent orogens. Geol. Soc. Am. Spec. Paper 541, 1–20. 10.1130/2018.2541(09).

Dörr, N., Lisker, F., Piepjohn, K., Spiegel, C., 2019. Cenozoic development of northern Svalbard based on thermochronological data. Terra Nova 31, 306–315. https://doi.org/10.1111/ter.12402.

Døssing, A., Japsen, P., Watts, A.B., Nielsen, T., Jokat, W., Thybo, H., Dahl-Jensen, T., 2016. Miocene uplift of the NE Greenland margin linked to plate tectonics: Seismic evidence from the Greenland Fracture Zone, NE Atlantic. Tectonics 35, 26 pp. https://doi.org/10.1002/2015TC004079.

Doubrovine, P.V., Steinberger, B., Torsvik, T.H., 2012. Absolute plate motions in a reference frame defined by moving hot spots in the Pacific, Atlantic, and Indian Oceans. J. Geoph. Res. 117 (B09101), 1–30. https://doi.org/10.1029/2011JB009072.

Dumais, M.-A., Gernigon, L., Olesen, O., Johansen, S.E., Brönner, M., 2021. New interpretation of the spreading evolution of the Knipovich Ridge derived from aeromagnetic data. Geophys. J. Int. 224, 1422–1428. https://doi.org/10.1093/gji/ggaa527.

Embry, A., Beauchamp, B., 2019. Sverdrup Basin. In: Miall, A.D. (Ed.), The Sedimentary Basins of the United States and Canada. Elsevier, New York, pp. 559–592. https://doi.org/10.1016/B978-0-444-63895-3.00014-0.

Embry, A., Beauchamp, B., Dewing, K., Dixon, J., 2018. Episodic tectonics in the Phanerozoic succession of the Canadian High Arctic and the "10-million-year flood". In: Piepjohn, K., Strauss, J.V., Reinhardt, L., McClelland, W.C. (Eds), Tectonic Evolution of the Arctic Margins and Trans-Arctic Links with Adjacent Orogens. GSA Special Publication 541, 213-230. 10.1016/B978-0-444-63895-3.00014-0.

Engen, Ø., Faleide, J.I., Dyreng, T.K., 2008. Opening of the Fram Strait gateway: A review of plate tectonic constraints. Tectonophysics 450, 51–69. https://doi.org/10.1016/j.tecto.2008.01.002.

Escher, J.C., Pulvertaft, T.C.R., 1995. Geological map of Greenland, 1:2 500 000. Geological Survey of Denmark, Copenhagen.

Evans, D. (Ed.), 2003. The Millennium Atlas: Petroleum Geology of the Central and Northern North Sea. London: Geological Society. 10.1017/s0016756803218124.

Faleide, J.I., Tsikalas, F., Breivik, A.J., Mjelde, R., Ritzmann, O., Engen, O., Wilson, J., Eldholm, O., 2008. Structure and evolution of the continental margin off Norway and the Barents Sea. Episodes 31, 82–91. 10.18814/epiiugs/2008/v31i1/012.

Fjellanger, E., Surlyk, F., Wamsteeker, L.C., Midtun, T., 2005. Upper Cretaceous basin-floor fans in the Vøring Basin, Mid-Norway shelf. In: Wandas, B. et al. (Eds), NPF Spec. Pub. 12, 135–164. 10.1016/S0928-8937(05)80047-5.

François, T., Koptev, A., Cloetingh, S., Burov, E., Gerya, T., 2018. Plume-lithosphere interactions in rifted margin tectonic settings: Inferences from thermo-mechanical modelling. Tectonophysics 746, 138–154. https://doi.org/10.1016/j.tecto.2017.11.027.

Fyhn, M.B., Hopper, J.R., Sandrin, A., Lauridsen, B.W., Heincke, B.H., Nøhr-Hansen, H., Andersen, M.S., Alsen, P., Nielsen, T., 2021. Three-phased latest Jurassic-Eocene rifting and mild mid-Cenozoic compression offshore NE Greenland. Tectonophysics 815,. https://doi.org/10.1016/j.tecto.2021.228990 228990.

Gaina, C., Gernigon, L., Ball, P., 2009. Palaeocene – Recent plate boundaries in the NE Atlantic and the formation of the Jan Mayen microcontinent. J. Geol. Soc. Lond. 166, 601–616. https://doi.org/10.1144/0016-76492008-112.

Gaina, C., Nasuti, A., Kimbell, G.S., Blischke, A., 2017. Break-up and seafloor spreading domains in the NE Atlantic. In: Péron–Pinvidic, G., Hopper, J.R., Stoker, M.S., Gaina, C., Doornenbal, J.C., Funck, T., Arting, U.E. (Eds), The NE Atlantic Region: A Reappraisal of Crustal Structure, Tectonostratigraphy and Magmatic Evolution. Geol. Soc., Lond., Spec. Publ. 447, 25 pp. 10.1144/SP447.12.

Gautier, D.L., Stemmerik, L., Christiansen, F.G., Sørensen, K., Bidstrup, T., Bojesen-Koefoed, J.A., Bird, K.J., Charpentier, R.R., Houseknecht, D.W., Klett, T.R., Scheck, C.J., Tennyson, M.E., 2011. Assessment of NE Greenland: prototype for development of Circum-Arctic Resource Appraisal methodology. In: Spencer, A.M., Embry, A.F., Gautier, D.L., Soupakova, A.V., Sørensen, K. (Eds) Arctic Petroleum Geology Memoirs 35, 663–672. London: Geological Society. 10.1144/M35.43.

Gill, R.C.O., Pedersen, A.K., Larsen, J.G., 1992. Tertiary picrites in West Greenland: melting at the periphery of a plume? In: Storey, B.C., Alabaster, T., Pankhusrst, R. J. (Eds), Magmatism and the Causes of Continental Break-up. Geol. Soc. Lond., Spec. Publ. 68, 335–348. 10.1144/GSL.SP.1992.068.01.21.

Gion, A.M., Williams, S.E., Mueller, R.D., 2017. A reconstruction of the Eurekan Orogeny incorporating deformation constraints. Tectonics 36, 304–320. https://doi.org/10.1002/2015tc004094.

Graham, D.W., Larsen, L.M., Storey, M., Pedersen, A.K., Lupton, J.E., 1998. Helium isotope composition of the early Iceland mantle plume inferred from the Tertiary picrites of West Greenland. Earth Planet. Sci. Lett. 160, 241–255. https://doi.org/10.1016/S0012-821X(98)00083-1.

Green, P.F., 2020. North Greenland and Svalbard: Thermal history reconstructions and tectonic development based on AFTA and VR data. Geotrack Report GC1231. Geotrack International, Victoria, Australia. 560 pp.

Green, P.F., Duddy, I.R., 2010. Synchronous exhumation events around the Arctic including examples from Barents Sea and Alaska North Slope. In: Vining, B.A., Pickering, S.C. (Eds), Petroleum Geology: From Mature Basins to New Frontiers – Proceedings of the 7th Petroleum Geology Conference. Geol. Soc., Lond., 633–644. 10.1144/0070633.

Green, P.F., Duddy, I.R. 2012: Thermal history reconstruction in sedimentary basins using apatite fission-track analysis and related techniques. In: Harris, N.B., Peters, K.E. (Eds), Analyzing the Thermal History of Sedimentary Basins: Methods and Case Studies, Soc. Sed. Geol. Mem. 103, 65–104. 10.2110/sepmsp.103.

Green, P., Duddy, I., 2018. Apatite (U-Th-Sm)/He thermochronology on the wrong side of the tracks. Chem. Geol. 488, 21–33. https://doi.org/10.1016/j.chemgeo.2018.04.028.

Green, P., Duddy, I., 2020. Discussion: Extracting thermal history from low temperature thermochronology. A comment on recent exchanges between Vermeesch and Tian and Gallagher and Ketcham. Earth-Sci. Rev. 103197. https://doi.org/10.1016/j.earscirev.2020.103197.

Green, P.F., Lidmar-Bergström, K., Japsen, P., Bonow, J.M., Chalmers, J.A. 2013. Stratigraphic landscape analysis, thermochronology and the episodic development of elevated passive continental margins. Geol. Surv. Denm. Greenl. Bull. 2013/30, 150 pp. 10.34194/geusb.v30.4673.

Green, P.F., Japsen, P., Guarnieri, P., Nielsen, T.F.D., 2014. Thermal history of outcrop samples from South-East Greenland based on apatite fission-track analysis, in: Stensgaard, B.M. (Ed.), South-East Greenland Mineral Endowment Task (SEGMENT), 2014 Workshop Abstract Volume. South-East Greenland Workshop, March 27–28 2014, Copenhagen, GEUS Report 2014/79, 21–25.

Green, P.F., Duddy, I.R., Japsen, P. 2018b. Multiple episodes of regional exhumation and inversion identified in the UK Southern North Sea based on integration of palaeothermal and palaeoburial indicators. Petroleum Geology Conference series 2018, 47–65. London: Geological Society. 10.1144/PGC8.21.

Green, P., Duddy, I., Japsen, P., 2022a. Episodic kilometre-scale burial and exhumation and the importance of missing section. Earth-Science Reviews 104226. https://doi.org/10.1016/j.earscirev.2022.104226.

Green, P.F., Japsen, P., Bonow, J.M., Chalmers, J.A., Duddy, I.R., Kukkonen, I., 2022b. The post-Caledonian thermo-tectonic evolution of Fennoscandia. Gondwana Res. 107, 201–234. https://doi.org/10.1016/j.gr.2022.03.007.

Green, P.F., Japsen, P., Chalmers, J.A., Bonow, J.M., Duddy, I.R., 2018a. Post-breakup burial and exhumation of passive continental margins: Seven propositions to inform geodynamic models. Gondwana Res. 53, 58–81. https://doi.org/10.1016/j.gr.2017.03.007.

Gregersen, U., Knutz, P.C., Nøhr-Hansen, H., Sheldon, E., Hopper, J.R., 2019. Tectonostratigraphy and evolution of the West Greenland continental margin. Bull. Geol. Soc. Denm. 67, 1–21. https://doi.org/10.37570/bgsd-2019-67-01.

Håkansson, E., Pedersen, S.A.S., 1982. Late Paleozoic to Tertiary tectonic evolution of the continental margin in North Greenland. Can. Soc. Pet. Geol. Mem. 8, 331–348.

Håkansson, E., Pedersen, S.A.S., 2015. A healed strike-slip plate boundary in North Greenland indicated through associated pull-apart basins. In: Gibson, B.S., Roure, F., Manatschal, G. (Eds), Sedimentary Basins and Crustal Processes at Continental Margins: From Modern Hyper-extended Margins to Deformed Ancient Analogues. Geol. Soc., Lond., Spec. Publ. 413, 143–169. 10.1144/sp413.10.

Håkansson, E., Stemmerik, L., 1989. Wandel Sea basin — A new synthesis of the late Paleozoic to Tertiary accumulation in North Greenland. Geology 17, 683–686. https://doi.org/10.1130/0091-7613(1989)017<0683:WSBANS>2.3.CO;2.

Harland, W.B. 1969. Contribution of Spitsbergen to Understanding of Tectonic Evolution of North Atlantic Region. In: Kay, M. (Ed.), North Atlantic. Geology and continental drift. A symposium. AAPG Memoir 12, 817–851.

Harrison, J.C., 2004. In search of the Wegener fault: re-evaluation of strike-slip displacements along and bordering nares strait. Polarforschung 74, 129–160.

Harrison, J.C., 2008. Regional variation in structural style, deformation kinematics, and summary of tectonic history, northeast Ellesmere Island. Bull. Geol. Surv. Canada 592, 245–284.

Harrison, C., St-Onge, M.R., 2022. Geological history and supercontinent cycles of the Arctic. GSA Bull. https://doi.org/10.1130/B36398.1.

Harrison, J.C., Mayr, U., McNeil, D.H., Sweet, A.R., McIntyre, D.J., Eberle, J.J., Harington, C.R., Chalmers, J.A., Dam, G., Nøhr-Hansen, H., 1999. Correlation of Cenozoic sequences of the Canadian Arctic region and Greenland; implications for the tectonic history of northern North America. Bull. Can. Petr. Geol. 47, 223–254. https://doi.org/10.35767/gscpgbull.47.3.223.

Heilmann-Clausen, C., Nielsen, O.B., Gersner, F., 1985. Lithostratigraphy and depositional environments in the upper Paleocene and Eocene of Denmark. Bull. Geol. Soc. Denm. 33, 287–323.

Helland-Hansen, W., Grundvåg, S.A., 2020. The Svalbard Eocene-Oligocene (?) Central Basin succession: Sedimentation patterns and controls. Basin Res. 33, 729–753. https://doi.org/10.1111/bre.12492.

Henriksen, E., Bjørnseth, H., Hals, T., Heide, T., Kiryukhina, T., Kløvjan, O., Larssen, G., Ryseth, A., Rønning, K., Sollid, K., 2011. Uplift and erosion of the greater Barents Sea: impact on prospectivity and petroleum systems. Geol. Soc., Lond Mem. 35, 271–281. https://doi.org/10.1144/M35.17.

Höink, T., Lenardic, A., Richards, M., 2012. Depth-dependent viscosity and mantle stress amplification. Implications for the role of the asthenosphere in maintaining plate tectonics. Geoph. J. Int. 191, 30–41. https://doi.org/10.1111/j.1365-246X.2012.05621.x.

Holford, S.P., Green, P.F., Hillis, R.R., Underhill, J.R., Stoker, M.S., Duddy, I.R., 2010. Multiple post-Caledonian exhumation episodes across NW Scotland revealed by apatite fission-track analysis. J. Geol. Soc Lond. 167, 675–694. https://doi.org/10.1144/0016-76492009-167.

Hopper, J.R., Funck, T., Stoker, M., Arting, U., Peron-Pinvidic, G., Doornenbal, H., Gaina, C., 2014. Tectonostratigraphic Atlas of the North-East Atlantic Region. Geological Survey of Denmark and Greenland, Copenhagen.

Horni, J.A., Hopper, J.R., Blischke, A., Geisler, W.H., Stewart, M., McDermott, K., Judge, M., Erlendsson, Ö., Árting, U., 2017. Regional distribution of volcanism within the North Atlantic Igneous Province. Geol. Soc., Lond Spec. Publ. 447, 105–125. https://doi.org/10.1144/SP447.18.

Hovikoski, J., Pedersen, G.K., Alsen, P., Lauridsen, B.W., Svennevig, K., Nøhr-Hansen, H., Sheldon, E., Dybkjær, K., Bojesen-Koefoed, J., Piasecki, S., 2018. The Jurassic–Cretaceous lithostratigraphy of Kilen, Kronprins Christian Land, eastern North Greenland. Bull. Geol. Soc. Denm. 66, 61–112. 10.37570/ bgsd-2018-66-04.

Iaffaldano, G., DeMets, C., 2016. Late Neogene changes in North America and Antarctica absolute plate motions inferred from the Mid-Atlantic and Southwest Indian Ridges spreading histories. Geophys. Res. Lett. 43, 8466–8472. https://doi.org/10.1002/2016GL070276.

Ineson, J.R., Hovikoski, J., Sheldon, E., Piasecki, S., Alsen, P., Fyhn, M.B., Bjerager, M., Dybkjær, K., Guarnieri, P., Lauridsen, B.W., 2020. Regional impact of Early Cretaceous tectono-magmatic uplift in the Arctic: implications of new data from eastern North Greenland. Terra Nova 9, pp. https://doi.org/10.1111/ter.12514.

Japsen, P., Green, P.F., Chalmers, J.A., 2005. Separation of Palaeogene and Neogene uplift on Nuussuaq, West Greenland. J. Geol. Soc Lond. 162, 299–314. https://doi.org/10.1144/0016-764904-038.

Japsen, P., Bonow, J.M., Green, P.F., Chalmers, J.A., Lidmar-Bergström, K., 2006. Elevated, passive continental margins: Long-term highs or Neogene uplifts? New evidence from West Greenland. Earth Planet. Sci. Lett. 248, 315–324. https://doi.org/10.1016/j.epsl.2006.05.036.

Japsen, P., Green, P.F., Nielsen, L.H., Rasmussen, E.S., Bidstrup, T., 2007. Mesozoic-Cenozoic exhumation events in the eastern North Sea Basin: a multi-disciplinary study based on palaeothermal, palaeoburial, stratigraphic and seismic data. Basin Res. 19, 451–490. https://doi.org/10.1111/j.1365-2117.2007.00329.x.

Japsen, P., Green, P.F., Bonow, J.M., Rasmussen, E.S., Chalmers, J.A., Kjennerud, T., 2010. Episodic uplift and exhumation along North Atlantic passive margins: implications for hydrocarbon prospectivity. In: Vining, B.A., Pickering, S.C. (Eds), Petroleum Geology: From Mature Basins to New Frontiers – Proceedings of the 7th Petroleum Geology Conference, 979–1004. London: Geological Society. 10.1144/0070979.

Japsen, P., Green, P.F., Bonow, J.M., Nielsen, T.F.D., Chalmers, J.A., 2014. From volcanic plains to glaciated peaks: Burial and exhumation history of southern East Greenland after opening of the North-East Atlantic. Glob. Planet. Change 116, 91–114. https://doi.org/10.1016/j.gloplacha.2014.01.012.

Japsen, P., Green, P.F., Bonow, J.M., Erlström, M., 2016. Episodic burial and exhumation of the southern Baltic Shield: epeirogenic uplifts during and after break-up of Pangea. Gondwana Res. 35, 357–377. https://doi.org/10.1016/j.gr.2015.06.005.

Japsen, P., Green, P.F., Chalmers, J.A., Bonow, J.M., 2018. Mountains of southernmost Norway: uplifted Miocene peneplains and re-exposed Mesozoic surfaces. J. Geol. Soc. Lond. 157, 721–741. https://doi.org/10.1144/jgs2017-157.

Japsen, P., Green, P.F., Chalmers, J.A., 2021a. Thermo-tectonic history of the Wandel Sea Basin, North Greenland. Geol. Surv. Denm. Greenl. Bull. 45, 41–83. https://doi.org/10.34194/geusb.v45.5298.

Japsen, P., Green, P.F., Bonow, J.M., Bjerager, M., Hopper, J.R. 2021b. Episodic burial and exhumation in North-East Greenland before and after opening of the North-East Atlantic. Geol. Surv. Denm. Greenl. Bull. 45, 162 pp. 10.34194/geusb.v45.5299.

Johannessen, E.P., Henningsen, T., Bakke, N.E., Johansen, T.A., Ruud, B.O., Riste, P., Elvebakk, H., Jochmann, M., Elvebakk, G., Woldengen, M.S., 2011. Palaeogene clinoform succession on Svalbard expressed in outcrops, seismic data, logs and cores. First Break 29, 35–44. https://doi.org/10.3997/1365-2397.2011004.

Jokat, W., Lehmann, P., Damaske, D.N., 2016. Magnetic signature of North-East Greenland, the Morris Jesup Rise, the Yermak Plateau, the central Fram Strait: Constraints for the rift/drift history between Greenland and Svalbard since the Eocene. Tectonophysics 691, 98–109. https://doi.org/10.1016/j.tecto.2015.12.002.

Jones, M.T., Augland, L.E., Shephard, G.E., Burgess, S.D., Eliassen, G.T., Jochmann, M. M., Friis, B., Jerram, D.A., Planke, S., Svensen, H.H., 2017. Constraining shifts in North Atlantic plate motions during the Palaeocene by U-Pb dating of Svalbard tephra layers. Sci. Rep. 7, 1–9. https://doi.org/10.1038/s41598-017-06170-7.

Koptev, A., Cloetingh, S., Ehlers, T.A., 2021. Longevity of small-scale ('baby') plumes and their role in lithospheric break-up. Geoph. J. Int. 227, 439–471. https://doi.org/10.1093/gji/ggab223.

Knies, J., Gaina, C., 2008. Middle Miocene ice sheet expansion in the Arctic: Views from the Barents Sea. Geochem. Geophys. Geosyst. 9. https://doi.org/10.1029/2007GC001824.

Knudsen, C., Hopper, J.R., Bierman, P.R., Bjerager, M., Funck, T., Green, P.F., Ineson, J. R., Japsen, P., Marcussen, C., Sherlock, S.C., Thomsen, T.B., 2017. Samples from the Lomonosov Ridge place new constraints on the geological evolution of the Arctic Ocean. In: Peace, V., Coakley, B. (Eds), Circum-Arctic Lithosphere Evolution. Geol. Soc., Lond., Spec. Publ. 460, 22 pp. 10.1144/sp460.17.

Larsen, R.B., Tegner, C., 2006. Pressure conditions for the solidification of the Skaergaard intrusion: Eruption of East Greenland flood basalts in less than 300,000 years. Lithos 92, 181–197. https://doi.org/10.1016/j.lithos.2006.03.032.

Larsen, M., Whitham, A., 2005. Evidence for a major sediment input point into the Faroe–Shetland Basin from the Kangerlussuaq region of southern East Greenland. In: Doré, A.G., Vining, B. (Eds), Petroleum Geology: North-West Europe and Global Perspectives—Proceedings of the 6th Petroleum Geology Conference, 913–922. London: Geological Society. 10.1144/0060913.

Larsen, L.M., Williamson, M.-C., 2020. Depleted and ultra-depleted basalt and picrite in the Davis Strait: Paleocene volcanism associated with a transform continental margin. Geol. Mag. 157, 1983–2003. https://doi.org/10.1017/S0016756820000175.

Lawver, L.A., Müller, R.D., 1994. Iceland hotspot track. Geology 22, 311–314.

Lowell, J.D., 1972. Spitsbergen Tertiary orogenic belt and the Spitsbergen Fracture Zone. Geol. Soc. Am. Bull. 83, 3091–3102.

Lyck, J.M., Stemmerik, L., 2000. Palynology and depositional history of the Paleocene? Thyra Ø Formation, Wandel Sea Basin, eastern North Greenland. Geol. Greenl. Surv. Bull. 187, 21–49. https://doi.org/10.34194/ggub.v187.5193.

Manby, G., Lyberis, N., 1996. State of stress and tectonic evolution of the West Spitsbergen Fold Belt. Tectonophysics 267, 1–29. https://doi.org/10.1016/S0040-1951(96)00109-6.

Manum, S.B., Throndsen, T., 1977. Rank of coal and dispersed organic matter and its geological bearing in the Spitsbergen Tertiary. Norsk Polarinstitutt Årbok 1977, 159–177.

Marshall, C., Uguna, J., Large, D.J., Meredith, W., Jochmann, M., Friis, B., Vane, C., Spiro, B.F., Snape, C.E., Orheim, A., 2015. Geochemistry and petrology of Paleocene coals from Spitzbergen—Part 2: Maturity variations and implications for local and regional burial models. Int. J. Coal Geol. 143, 1–10. https://doi.org/10.1016/j.coal.2015.03.013.

Matthews, K.J., Maloney, K.T., Zahirovic, S., Williams, S.E., Seton, M., Mueller, R.D., 2016. Global plate boundary evolution and kinematics since the late Paleozoic. Glob. Planet. Change 146, 226–250. https://doi.org/10.1016/j.gloplacha.2016.10.002.

Merkouriev, S., DeMets, C., 2008. A high-resolution model for Eurasia-North America plate kinematics since 20 Ma. Geoph. J. Int. 173, 1064–1083. https://doi.org/10.1111/j.1365-246X.2008.03761.x.

Nielsen, T.F.D., Soper, N.J., Brooks, C.K., Faller, A.M., Higgins, A.K., Matthews, D.W., 1981. The pre-basaltic sediments and the Lower Basalts at Kangerdlgssuaq, East Greenland: their stratigraphy, lithology, palaeomagnetism and petrology. Meddelelser om Grønland, Geoscience 6, 1–25.

Nøhr-Hansen, H., Nielsen, L.H., Sheldon, E., Hovikovski, J., Alsen, P., 2011. Palaeogene deposits in north-east Greenland. Bull. Geol. Surv. Denm. Greenl. 23, 61–64. https://doi.org/10.34194/geusb.v23.4867.

Nøttvedt, A., Johannessen, E.P., Surlyk, F. 2008. The Mesozoic of western Scandinavia and East Greenland. Episodes J. Int. Geosci. 31, 59–65. 10.18814/epiiugs/2008/v31i1/009.

O'Neill, C., Müller, D., Steinberger, B., 2005. On the uncertainties in hot spot reconstructions and the significance of moving hot spot reference frames. Geochem Geophys 6. https://doi.org/10.1029/2004GC000784.

Oakey, G.N., Chalmers, J.A., 2012. A new model for the Paleogene motion of Greenland relative to North America: Plate reconstructions of the Davis Strait and Nares Strait regions between Canada and Greenland. J. Geoph. Res. - Solid Earth 117, 1–28. https://doi.org/10.1029/2011jb008942.

Oakey, G.N., Chalmers, J.A., 2013. Reply to comment by Denyszyn and Halls on "Geological and geophysical observations in the Kane Basin preclude the presence of a major plate boundary in southwestern Nares Strait". J. Geoph. Res. Solid Earth 119, 2539–2542 https://doi:10.1002/2013JB010323.

Oakey, G.N., Damaske, D., 2006. Continuity of basement structures and dyke swarms in the Kane Basin region of central Nares Strait con-strained by aeromagnetic data. Polarforschung 74, 51–62.

Ogg, J.G. 2020. Geomagnetic polarity time scale. In: Gradstein, F., Ogg, J.G., Schmitz, M., Ogg, G.M. (Eds): Geologic time scale 2020, 159–192. Elsevier. 10.1016/B978-0-12-824360-2.00005-X.

Olaussen, S., Larssen, G.B., Helland-Hansen, W., Johannessen, E.P., Nøttvedt, A., Riis, F., Rismyhr, B., Smelror, M., Worsley, D., 2018. Mesozoic strata of Kong Karls Land, Svalbard, Norway; a link to the northern Barents Sea basins and platforms. Norwegian Journal of Geology/Norsk Geologisk Forening 98.

Olaussen, S., Grundvåg, S.-A., Senger, K., Anell, I., Betlem, P., Birchall, T., Braathen, A., Dallmann, W., Jochmann, M., Johannessen, E.P. 2022. The Svalbard Carboniferous to Cenozoic Composite Tectono-Stratigraphic Element. In: Drachev, S.S, Brekke, H., Henriksen, E., Moore, T. (Eds), Sedimentary Successions of the Arctic Region and their Hydrocarbon Prospectivity. Geol. Soc., Lond., Mem. 57, M57-2021-36. 10.1144/M57-2021-36.

Paech, H.-J., Koch, J., 2001. Coalification in post-Caledonian sediments on Spitsbergen. Geologisches Jahrbuch, Reihe B, pp. 507–534.

Pedersen, A.K., Larsen, L.M., Dueholm, K.S., 1993. Geological section along the south coast of Nuussuaq, central West Greenland. 000 coloured geological sheet, 1. Grønlands Geologiske Undersøgelse, Copenhagen, p. 20.

Pedersen, A.K., Larsen, L.M., Riisager, P., Dueholm, K.S., 2002. Rates of volcanic deposition, facies changes and movements in a dynamic basin: the Nuussuaq Basin, West Greenland, around the C27n-C26R transition. In: Jolley, D.W., Bell, B.R. (Eds), The North Atlantic Igneous Province: Stratigraphy, Tectonic, Volcanic and Magmatic Processes. Geol. Soc., Lond., Spec. Publ. 197, 157–181. 10.1144/GSL.SP.2002.197.01.07.

Pedersen, A.K., Larsen, L.M., Pedersen, G.K., 2017. Lithostratigraphy, geology and geochemistry of the volcanic rocks of the Vaigat formation on Disko and Nuussuaq, Paleocene of West Greenland. Geol. Surv. Denm. Greenl. Bull. 39, 247 pp.

Pedersen, G.K., Lauridsen, B.W., Svennevig, K., Bojesen-Koefoed, J.A., Nøhr-Hansen, H., Alsen, P., 2018. Burial history of a folded cretaceous succession–A case study from the southern part of Kilen, eastern north Greenland. Cret. Res. 89, 22–35. https://doi.org/10.1016/j.cretres.2018.03.007.

Péron-Pinvidic, G., Hopper, J. R., Stoker, M. S., Gaina, C., Doornenbal, J. C., Funck, T. and Árting, U. E. (Eds) 2017. The NE Atlantic Region: A Reappraisal of Crustal Structure, Tectonostratigraphy and Magmatic Evolution. Geol. Soc., Lond., Spec. Publ. 447. 457 pp. 10.1144/SP447.17.

Piasecki, S., Nøhr-Hansen, H., Dalhoff, F., 2018. Revised stratigraphy of Kap Rigsdagen beds, Wandel Sea Basin, North Greenland. Newsletters on Stratigraphy 51, 411–425. https://doi.org/10.1127/nos/2018/0444.

Piepjohn, K., von Gosen, W., 2001. Polyphase deformation at the Harder Fjord Fault Zone (North Greenland). Geol. Mag. 138, 407–434. https://doi.org/10.1017/s0016756801005660.

Piepjohn, K., Gosen, W. von, Tessensohn, F., Reinhardt, L., McClelland, W. C., Dallmann, W., Gaedicke, C., Harrison, J. C., 2015. Tectonic map of the Ellesmerian and Eurekan deformation belts on Svalbard, North Greenland, and the Queen Elizabeth Islands (Canadian Arctic), arktos 1, 1–7, 10.1007/s41063-015-0015-7.

Piepjohn, K., von Gosen, W., Tessensohn, F., 2016. The Eurekan deformation in the Arctic: an outline. J. Geol. Soc Lond. 173, 1007–1024. https://doi.org/10.1144/jgs2016-081.

Pulvertaft, T.C.R., Dawes, P.R., 2011. North Atlantic spreading axes terminate in the continental cul-de-sacs of Baffin Bay and the Laptev Sea. Can. J. Earth Sci. 48, 593–601. https://doi.org/10.1139/E11-004.

Ricketts, B.D., 1994. Basin analysis, Eureka Sound Group, Axel Heiberg and Ellesmere Islands, Canadian Arctic archipelago. Geol. Surv. Can. Mem. 439, 119 pp. https://doi.org/10.4095/194814.

Ricketts, B.D., Stephenson, R.A., 1994. The demise of Sverdrup Basin; Late Cretaceous-Paleogene sequence stratigraphy and forward modeling. J. Sed. Res. 64, 516–530. https://doi.org/10.1306/D4267FF5-2B26-11D7-8648000102C1865D.

Riisager, J., Riisager, P., Pedersen, A.K., 2003. The C27n–C26r geomagnetic polarity reversal recorded in the west Greenland flood basalt province: How complex is the transitional field? J. Geophys. Res. 108 (B3) 2155, 11 pp. https://doi.org/10.1029/2002JB002124.

Roest, W.R., Srivastava, S.P., 1989. Sea-floor spreading in the Labrador Sea. a new reconstruction. Geology 17, 1000–1003. https://doi.org/10.1130/0091-7613(1989)017<1000:SFSITL>2.3.CO;2.

Sømme, T.O., Skogseid, J., Løseth, H., Embry, P., 2019. Manifestation of tectonic and climatic perturbations in deep-time stratigraphy–an example from the Paleocene succession offshore western Norway. Frontiers Earth Sci. 7, 1–20. https://doi.org/10.3389/feart.2019.00303.

Srivastava, S.P., 1978. Evolution of the Labrador Sea and its bearing on the early evolution of the North Atlantic. Geophys. J. R. Astron. Soc. 52, 313–357. https://doi.org/10.1111/j.1365-246X.1978.tb04235.x.

Srivastava, S.P., Keen, C.E., 1995. A deep seismic reflection profile across the extinct mid-Labrador Sea spreading center. Tectonics 14, 372–389. https://doi.org/10.1029/94TC02453.

Steel, R., Gjelberg, J., Helland-Hansen, W., Kleinspehn, K., Nøttvedt, A., Rye-Larsen, M., 1985. The Tertiary strike-slip basins and orogenic belt of Spitsbergen. In: Biddle, K.T., Christle-Blick. K. (Eds), Strike-Slip Deformation, Basin Formation, and Sedimentation. Soc. Econ. Paleont. Mineral. (SEPM) Spec. Publ. 37, 339–359. 10.2110/pec.85.37.0339.

Stemmerik, L., Worsley, D., 2005. 30 years on-Arctic Upper Palaeozoic stratigraphy, depositional evolution and hydrocarbon prospectivity. Norw. J. Geol. 85, 151–168.

Stemmerik, L., Dalhoff, F., Larsen, B.D., Lyck, J.M., Mathiesen, A., Nilsson, I., 1998. Wandel Sea Basin, eastern North Greenland. Bull. Geol. Surv. Greenland 180, 55–62.

Stephenson, R., Ricketts, B., Cloetingh, S., Beekman, F., 1990. Lithosphere folds in the Eurekan orogen, Arctic Canada? Geology 18, 603–606. https://doi.org/10.1130/0091-7613(1990)018<0603:LFITEO>2.3.CO;2.

Stoker, M.S., Stewart, M.A., Shannon, P.M., Bjerager, M., Nielsen, T., Blischke, A., Hjelstuen, B., Gaina, C., McDermott, K., Ólavsdóttir, J., 2017. An overview of the Upper Palaeozoic–Mesozoic stratigraphy of the NE Atlantic region. In: Péron-Pinvidic, G., Hopper, J.R., Stoker, M.S., Gaina, C., Doornenbal, J.C., Funck, T., Àrting, U. E. (Eds), The NE Atlantic Region: A Reappraisal of Crustal Structure, Tectonostratigraphy and Magmatic Evolution. Geol. Soc., Lond., Spec. Publ. 447, 11–68. 10.1144/sp447.2.

Stotz, I.L., Iaffaldano, G., Davies, D.R., 2018. Pressure-Driven Poiseuille Flow: A Major Component in the Torque-Balance Governing Pacific Plate Motion. Geoph. Res. Lett. 45, 117–125. https://doi: 10.1002/2017GL075697.

Svennevig, K., Guarnieri, P., Stemmerik, L., 2016. Tectonic inversion in the Wandel Sea Basin: A new structural model of Kilen (eastern North Greenland). Tectonics 35, 2896–2917. https://doi.org/10.1002/2016TC004152.

Svennevig, K., Alsen, P., Guarnieri, P., Hovikoski, J., Lauridsen, B.W., Pedersen, G.K., Nøhr-Hansen, H., Sheldon, E., 2018. Descriptive text to the Geological map of Greenland, 1: 100 000, Kilen 81 Ø. 1 Syd. Geol. Surv. Denm. Greenl. Map Series 8, 1–29. 10.34194/geusm.v8.4526.

Tegner, C., Storey, M., Holm, P.M., Thorarinsson, S.B., Zhao, X., Lo, C.H., Knudsen, M.F., 2011. Magmatism and Eurekan deformation in the High Arctic Large Igneous Province: 40Ar-39Ar age of Kap Washington Group volcanics. North Greenland. Earth Planet. Sci. Lett. 303, 203–214. https://doi.org/10.1016/j.epsl.2010.12.047.

Tessensohn, F., Piepjohn, K., 2000. Eocene compressive deformation in Arctic Canada, North Greenland and Svalbard and its plate tectonic causes. Polarforschung 68, 21–124.

Thorsteinsson, R., Tozer, E.T. 1970. Geology of the Arctic Archipelago. In: Douglass, R.J.W. (Ed.), Geology and economic minerals of Canada. Geol. Survey Can. Econ. Geol. Rep. No. 1, 547–590.

Vamvaka, A., Pross, J., Monien, P., Piepjohn, K., Estrada, S., Lisker, F., Spiegel, C., 2019. Exhuming the top end of North America: episodic evolution of the Eurekan belt and its potential relationships to North Atlantic plate tectonics and Arctic climate change. Tectonics 4207–4228. https://doi.org/10.1029/2019tc005621.

von Gosen, W., Piepjohn, K., 2003. Eurekan transpressive deformation in the Wandel Hav Mobile Belt (northeast Greenland). Tectonics 22, 28 pp. https://doi.org/10.1029/2001TC901040.

von Gosen, W., Piepjohn, K., Gilotti, J.A., McClelland, W.C., Reinhardt, L., 2019. Structural evidence for sinistral displacement on the Wegener Fault in southern Nares Strait, Arctic Canada. In: Piepjohn, K., Strauss, J.V., Reinhardt, L., McClelland, W.C. (Eds), Circum-Arctic Structural Events: Tectonic Evolution of the Arctic Margins and Trans-Arctic Links with Adjacent Orogens: Geol. Soc. Am. Spec. Pap. 541, 367–396, 10.1130/2018.2541(18).

Wegener, A., 1912. Die Entstehung der Kontinente. Geol. Rundschau 3, 276–292.

White, N., Lovell, B., 1997. Measuring the pulse of a plume with the sedimentary record. Nature 387, 888–891. https://doi.org/10.1038/43151.

Wilson, J.T., 1965. A new class of faults and their bearing on continental drift. Nature 207, 343–347. https://doi.org/10.1038/207343a0.